2014

Protein/Protein Interactions in the Mammalian Heme Degradation Pathway *HEME OXYGENASE-2, CYTOCHROME P450 REDUCTASE, AND BILIVERDIN REDUCTASE*

Andrea L. M. Spencer
University of Michigan, Ann Arbor

Ireena Bagai
University of Michigan, Ann Arbor, ireena.bagai@gmail.com

Donald F. Becker
University of Nebraska-Lincoln, dbecker3@unl.edu

Erik R. P. Zuiderweg
University of Michigan, Ann Arbor, zuiderwe@umich.edu

Stephen W. Ragsdale
University of Michigan, Ann Arbor, sragsdal@umich.edu

THE JOURNAL OF BIOLOGICAL CHEMISTRY VOL. 289, NO. 43, pp. 29836–29858, October 24, 2014

Protein/Protein Interactions in the Mammalian Heme Degradation Pathway

*HEME OXYGENASE-2, CYTOCHROME P450 REDUCTASE, AND BILIVERDIN REDUCTASE**

Received for publication, May 18, 2014, and in revised form, August 18, 2014 Published, JBC Papers in Press, September 7, 2014, DOI 10.1074/jbc.M114.582783

Andrea L. M. Spencer[‡], Ireena Bagai[§1], Donald F. Becker[¶], Erik R. P. Zuiderweg[§2], and Stephen W. Ragsdale[‡§3]

From the [‡]Cellular and Molecular Biology Training Program and [§]Department of Biological Chemistry, University of Michigan, Ann Arbor, Michigan 48103 and the [¶]Department of Biochemistry, University of Nebraska-Lincoln, Lincoln, Nebraska 68588

Background: Heme oxygenase, cytochrome P450 reductase, and biliverdin reductase are the key enzymes in heme degradation.
Results: Specific electrostatic and hydrophobic interactions form the binding interface between heme oxygenase and cytochrome P450 reductase.
Conclusion: Heme oxygenase binds cytochrome P450 reductase dynamically and biliverdin reductase very weakly.
Significance: Characterizing interactions among proteins involved in heme degradation are crucial to understanding heme homeostasis.

Heme oxygenase (HO) catalyzes the rate-limiting step in the O_2-dependent degradation of heme to biliverdin, CO, and iron with electrons delivered from NADPH via cytochrome P450 reductase (CPR). Biliverdin reductase (BVR) then catalyzes conversion of biliverdin to bilirubin. We describe mutagenesis combined with kinetic, spectroscopic (fluorescence and NMR), surface plasmon resonance, cross-linking, gel filtration, and analytical ultracentrifugation studies aimed at evaluating interactions of HO-2 with CPR and BVR. Based on these results, we propose a model in which HO-2 and CPR form a dynamic ensemble of complex(es) that precede formation of the productive electron transfer complex. The ^{1}H-^{15}N TROSY NMR spectrum of HO-2 reveals specific residues, including Leu-201, near the heme face of HO-2 that are affected by the addition of CPR, implicating these residues at the HO/CPR interface. Alanine substitutions at HO-2 residues Leu-201 and Lys-169 cause a respective 3- and 22-fold increase in K_m values for CPR, consistent with a role for these residues in CPR binding. Sedimentation velocity experiments confirm the transient nature of the HO-2·CPR complex (K_d = 15.1 μM). Our results also indicate that HO-2 and BVR form a very weak complex that is only captured by cross-linking. For example, under conditions where CPR affects the ^{1}H-^{15}N TROSY NMR spectrum of HO-2, BVR has no effect. Fluorescence quenching experiments also suggest that BVR binds HO-2 weakly, if at all, and that the previously reported high affinity of BVR for HO is artifactual, resulting from the effects of free heme (dissociated from HO) on BVR fluorescence.

Precise regulation of heme metabolism is crucial for the cell. Heme is an active catalyst for generating reactive oxygen species by Fenton chemistry and is cytotoxic at elevated levels (above ~1 μM) (1). Heme is also a required prosthetic group for many proteins involved in electron transfer, oxygen transport, and redox enzymology (*e.g.* oxidases) (2). The mammalian heme degradation pathway consists of two enzymatic steps, which are mediated by heme oxygenase (HO)[4] and biliverdin reductase (BVR) (Fig. 1). Cytochrome P450 reductase (CPR) is required as an electron donor for HO catalysis. HO is the only known catalyst in the mammalian cell that degrades heme (Reaction 1). HO catalyzes the conversion of heme to biliverdin in a reaction that requires O_2, NADPH, and CPR, which transfers seven electrons as shown in Reaction 1 (3, 4). BVR then converts biliverdin to bilirubin (Reaction 2), which undergoes conjugation with glucuronate and is excreted from the body.

$$\text{heme} + 7e^- + 3O_2 \rightarrow \text{biliverdin} + CO + Fe(II) + 3H_2O$$
REACTION 1

$$\text{biliverdin} + 2e^- \rightarrow \text{bilirubin}$$
REACTION 2

In addition to protecting the cell from the toxicity of free heme, the heme degradation pathway generates biologically important products. The HO reaction is the only cellular source of CO, and although high levels of CO are toxic (>500 ppm), at

* This work was supported, in whole or in part, by National Institutes of Health Grants HL 102662A (to S. W. R.) and P30GM103335 and GM061068 (to D. B.). This work was also supported by National Science Foundation Grant DBI-0619764 (to D. B.). The stipend for A. L. M. S. was supported in part by National Institutes of Health Grant T32GM007215.

[1] Present address: Dept. of Neurology, Weill Medical College of Cornell University, New York, NY 10021.
[2] To whom correspondence may be addressed: Dept. of Biological Chemistry, University of Michigan Medical School, 1150 W. Medical Center Dr., 5301 MSRB III, Ann Arbor, MI 48109-0606. Tel.: 734-276-4463; Fax: 734-763-4581; E-mail: zuiderwe@umich.edu.
[3] To whom correspondence may be addressed: Dept. of Biological Chemistry, University of Michigan Medical School, 1150 W. Medical Center Dr., 5301 MSRB III, Ann Arbor, MI 48109-0606. Tel.: 734-615-4621; Fax: 734-763-4581; E-mail: sragsdal@umich.edu.

[4] The abbreviations used are: HO, heme oxygenase; CPR, cytochrome P450 reductase; BVR, biliverdin reductase; TROSY, transverse relaxation-optimized spectroscopy; SPR, surface plasmon resonance; LC-SPDP, succinimidyl 6-(3-[2-pyridyldithio]-propionamido)hexanoate; CPM, 7-diethylamino-3-(4′-maleimidylphenyl)-4-methylcoumarin; CSP, chemical shift perturbation; Ni-NTA, nickel-nitrilotriacetic acid; PDB, Protein Data Bank; SPR, surface plasmon resonance.

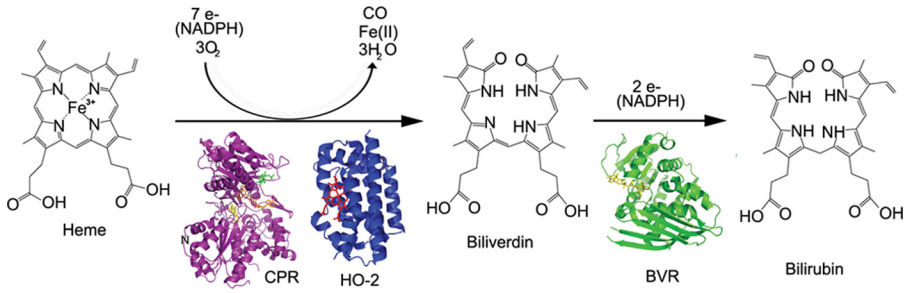

FIGURE 1. **Heme degradation pathway.** The two enzymatic steps of heme degradation mediated by heme oxygenase and biliverdin reductase. HO converts heme to biliverdin, and BVR converts biliverdin to bilirubin. The HO reaction requires electrons transferred from NADPH via cytochrome P450 reductase (PDB 1AMO, 2QPP, and 2H63).

low levels, CO acts as a signaling molecule akin to NO (5, 6) and is cytoprotective (7). The release and recycling of iron from heme is critical for iron homeostasis as most of the iron required for the synthesis of new ferroproteins and heme comes from recycled iron, with less than 3% of the daily iron requirement derived from the diet (2, 8). Finally, the HO system protects cells against oxidative stress, both by controlling free heme levels and by producing bilirubin, a potent antioxidant (9–11).

The heme degradation pathway affects many areas of cellular health as follows: heme and iron homeostasis, antioxidant protection, and gaseous signaling. As such, it is crucial to understand the mechanisms that regulate the activity of HO.

HO exists as two major isoforms, HO-1 and HO-2. HO-3 has also been described; however, it has low catalytic activity, and its biologic role and relevance are uncertain (12, 13). HO-1 and HO-2 share a high degree of homology (55% identity and 76% similarity) and display similar enzymatic activity (14). The two isoforms, however, have distinct patterns of expression and regulation. HO-1 is transcriptionally regulated and is expressed in most tissues, whereas HO-2 is constitutively expressed in a narrow range of tissues, primarily the brain and testes (15). Both HOs possess C-terminal membrane-spanning regions that tether them to the endoplasmic reticulum. However, because of poor solubility of the full-length protein, most enzymatic studies (as those described in this paper) have been conducted with a stable soluble form of HO lacking the C-terminal region. A major difference between the two HOs is that HO-2 contains three heme regulatory motifs, consisting of a Cys-Pro dyad, whereas HO-1 completely lacks cysteines (16). Two of these heme regulatory motifs are at the C terminus of HO-2, just preceding the membrane-spanning section. When these are in the dithiol state, the affinity of HO-2 for heme (relative to the disulfide state) decreases significantly, suggesting that the heme regulatory motifs act as a redox switch that controls activity in response to changes in cellular redox poise (17–19).

Electrons are transferred to HO from NADPH via the ~77-kDa dual flavin enzyme CPR through a pathway that involves its bound cofactors, FAD and FMN (20–23). In the cell, CPR is tethered to the endoplasmic reticulum by an N-terminal membrane-spanning region. Protein/protein interactions between the soluble forms of HO-1 and CPR and between HO-1 and BVR have been described *in vitro* (24–27) and are an aspect of regulation that has not been addressed for HO-2. CPR also forms electron transfer complexes with the cytochromes P450, cytochrome b_5, cytochrome *c*, and squalene monooxygenase (23, 28–31). Interactions with CPR may help define distinct roles for the HO isoforms. For example, recent reports suggest that binding of HO-1 and CPR regulates HO-1 nuclear translocation and the transcriptional regulatory response under hypoxia by stabilizing the endoplasmic reticulum-tethered form of HO-1 in the cell (32). However, HO-2 appears to remain stably associated at the endoplasmic reticulum irrespective of hypoxic challenge (32).

The complex between the soluble forms of CPR and HO-1 (lacking their membrane-spanning regions) has been characterized by fluorescence quenching (27), surface plasmon resonance (SPR) (24), and acetylation protection assays (25). These reports provide K_d values for the HO-1·CPR complex that range from 0.4 ± 0.1 to 2.4 ± 0.6 μM. CPR protects lysine residues 149 and 153 in HO-1 from chemical modification, suggesting that these basic residues are at the interface of the HO-1·CPR complex (25). Additionally, SPR studies indicate that the K149A substitution results in an ~10-fold increase in K_d for the HO-1·CPR complex (24). Although the HO-1·CPR complex has been relatively well characterized, the HO-2·CPR complex has not.

BVR catalyzes the second step in heme degradation, *i.e.* the reduction of biliverdin to bilirubin (Reaction 2). BVR is a soluble ~33-kDa protein that utilizes two electrons from either NADH or NADPH making it unique to have dual cofactor specificity at distinct pH values (33). In addition to its canonical enzymatic function, BVR has also been shown to bind and traffic heme to the nucleus where it regulates HO-1 expression (34–37). Also, BVR is a dual specificity (Ser/Thr and Tyr) kinase, and as such it is implicated in mitogen-activated protein kinase (MAPK) cell signaling pathways (38, 39).

Two groups have reported interactions between HO-1 and BVR via fluorescence quenching studies and SPR (24, 27). The fluorescence quenching studies suggest a high affinity HO-1·BVR complex ($K_d = 0.2$ μM) is formed, whereas SPR studies report that BVR competes with CPR for binding to HO-1. However, studies that identified the HO-1/CPR interface via lysine acetylation protection assays failed to find evidence for an HO-1/BVR interaction (25). Under single turnover conditions, the rate-limiting step of the HO-1 reaction is the release of biliverdin; however, in the presence of BVR, this step is accelerated (40), which indicates kinetic coupling between these two enzymes. Thus, although some evidence supports the formation of a high affinity complex between HO-1 and BVR,

other evidence challenges it. Furthermore, to our knowledge, the extent to which HO-2 is able to interact with BVR has not been addressed. Protein/protein interactions between HO and its reaction partners may play an important role in regulating its various properties, including cellular localization and enzymatic activity. Furthermore, given that they exhibit different modes of transcriptional regulation, HO-1 and constitutive HO-2 may differ in their affinity for BVR and CPR.

To gain insight into the protein level mode of regulating HO-2 activity, and to resolve some of the discrepancies related to measured interactions (or lack thereof) of HO-1 and HO-2 with their binding partners, we have performed nuclear magnetic resonance (NMR), kinetic, analytical ultracentrifugation, gel filtration, cross-linking, SPR, and fluorescence quenching studies. Our experiments indicate that both HO-1 and HO-2 form complexes with CPR. The interaction between HO-2 and BVR, however, is weak as compared with CPR, and it can only be detected by irreversible methods such as cross-linking. Our results allow us to propose an interface for the HO-2·CPR complex near the heme-binding face of HO-2 that includes residues Leu-201 and Lys-169. Furthermore, our studies demonstrate that the HO/CPR interface includes both hydrophobic and charge interactions. Our studies suggest a reinterpretation of protein/protein interactions in the heme degradation pathway. We demonstrate that both HO-1 and HO-2 bind CPR in a transient electron transfer complex that is required for HO activity. However, interactions between BVR and HO-2 are weak to undetectable and may not play a significant role in the physiologic context of a cell.

EXPERIMENTAL PROCEDURES

Materials—Ampicillin, isopropyl β-D-thiogalactopyranoside, kanamycin, NADPH, $NADP^+$, riboflavin, and hemin were purchased from Sigma. 7-Diethylamino-3-(4′-maleimidylphenyl)-4-methylcoumarin (CPM) was purchased from Molecular Probes, Inc. (Eugene, OR). OneShot® BL21(DE3) chemically competent cells were purchased from Invitrogen. Nickel-nitrilotriacetic acid (NTA) resin was from Qiagen (Valencia, CA). Glutathione-Sepharose was purchased from GE Healthcare.

Enzymes—Truncated versions of human $HO\text{-}1_{265}$ containing residues 1–265, and human $HO\text{-}2_{288}$ containing residues 1–288, and variants of these enzymes, were used in these studies. These enzymes lack the C-terminal amino acids that comprise their membrane anchors and will be referred to as HO-1 and HO-2. To facilitate expression, solubility, and ease of purification, HO-1 was cloned into the expression vector pMCSG10 by ligation-independent cloning (41). HO-2 was expressed and purified from the pET28a(+) vector. HO-1 and HO-2 were purified via an N-terminal His_6 tag using Ni-NTA affinity chromatography according to the manufacturer's guidelines (Qiagen, Valencia, CA).

Human $CPR_{\Delta 66}$ lacking the N-terminal membrane anchor was expressed from the pET28a(+) vector and is referred to as CPR for all studies described herein. CPR was expressed in BL21(DE3) cells and purified according to published methods (42). Human BVR was expressed from the pGEX-4T-2 vector and purified via glutathione-Sepharose affinity resin according to the manufacturer's instructions (GE Healthcare).

Unless stated otherwise, affinity purification tags were removed from all proteins by proteolysis before use in these experiments. Tobacco etch virus protease (expressed in *Escherichia coli* from pRK793, a derivative of BL21(DE3)-RIL, generously supplied by Dr. David S. Waugh at the Center for Cancer Research at NCI, National Institutes of Health) was used for HO-1, and thrombin was used for HO-2, CPR, and BVR. The affinity tags were separated from the protein by chromatography with the appropriate affinity resin (Ni-NTA for HO-1, HO-2, and CPR; and glutathione-Sepharose for BVR). All purification steps were performed at 4 °C.

The cDNA for human full-length HO-1 was graciously supplied by Dr. Ortiz de Montellano (University of California at San Francisco). The ligation-independent cloning expression vector pMCSG10 was donated by Dr. William Clay Brown (University of Michigan, Ann Arbor). Human full-length HO-2 cDNA in a pGEX-4T-2 vector was generously contributed by Dr. Mahin D. Maines (University of Rochester, School of Medicine, Rochester, NY) and was subcloned into the pET28a(+) expression vector. CPR was kindly donated by Dr. Bettie Sue Masters (University of Texas Health Sciences Center, Arlington, TX). The *BVR* gene was purchased from American Type Culture Collection (Manassas, VA) and subcloned into the pGEX-4T-2 plasmid.

Site-directed Mutagenesis of HO-1 and HO-2—Point mutations of HO-1 and HO-2 were constructed using the QuikChange site-directed mutagenesis protocol (Stratagene, La Jolla, CA). Oligonucleotides were synthesized by Integrated DNA Technologies (Coralville, IA). Positive transformants were enriched by antibiotic selection and confirmed using sequence analysis. All of the variants were purified exactly as described above for the wild type enzymes.

NMR Samples—BL21(DE3) cells containing the pET28a(+)/HO-2 plasmid were cultured in M9 minimal media with 1.0 g/liter $^{15}NH_4Cl$ (Cambridge Isotopes, Tewksbury, MA) to achieve ^{15}N labeling of the soluble HO-2 protein. HO-2 was purified as described above and loaded with heme by titration of freshly prepared hemin. Hemin stocks were prepared by solubilizing hemin in 15% dimethyl sulfoxide (DMSO), 0.1 M NaOH, 50 mM Tris, pH 7.0. Hemin stocks were centrifuged at 17,000 × *g* for 10 min at 4 °C, and the supernatant was then passed through a 0.22-micron filter (Millipore, Billerica, MA) to remove insoluble matter. Hemin concentration was determined using an $\Sigma_{385\ nm}$ of 58.44 mM^{-1} (43). HO-2 was loaded with hemin by titrating small amounts of hemin and monitoring the Soret peak at 404 nm until saturating levels of heme binding were achieved. NMR samples were prepared with 150 μM heme-bound HO-2 in 50 mM Tris-HCl, pH 7.0, 50 mM KCl with 10% D_2O in a total volume of 350 μl and placed in a Shigemi NMR tube. Experiments testing the ability of CPR or BVR to bind HO-2 were conducted with 150 μM HO-2 and the binding partner (BVR or CPR) at the indicated concentration.

$^1H\text{-}^{15}N$ apoHO-2 NMR TROSY samples were prepared identically to those described for hHO-2; however, heme was absent from the samples.

For perdeuterated ^{15}N-HO-2, samples were prepared as described above; however, BL21(DE3) cells were grown and induced in ^2H_2O/M9 minimal media. Electrospray ionization

mass spectrometry analysis revealed label incorporation to be 99.8%.

^{1}H-^{15}N TROSY NMR Measurements—Two-dimensional ^{1}H-^{15}N HSQC TROSY spectra were acquired on an Agilent/Varian 800 MHz spectrometer equipped with a triple resonance gradient (PFG) cryoprobe operating at 30 °C. Spectra were acquired using an array of 2404 × 300 complex points and with the spectral widths of 12019.2 and 2999.9 Hz for ^{1}H and ^{15}N, respectively. All spectra were processed with NMRPipe software (44) and visualized using Sparky 3.114 (45). Intensity analysis was conducted as described (46); the peak heights of chemical shifts were derived from Sparky and used to calculate the ratio of resonance height for the ^{1}H-^{15}N HO-2 spectrum with and without CPR or BVR. The chemical shift perturbation (CSP) for the assigned cross-peaks was measured between the 0 μM CPR spectrum and the 75 or 150 μM CPR spectrum for the perdeuterated ^{15}N-hHO-2 TROSY spectrum. CSPs were calculated from the square root of the sum of the squared N^{1}H and ^{15}N CSPs for each assigned cross-peak.

NMR Relaxation—The experiments for studying the ^{15}N NMR relaxation of HO-2 were carried out using a 40 μM HO-2 sample that was ^{15}N-labeled in 50 mM Tris-HCl, 50 mM KCl, pH 7.0, and recorded at 30 °C on a Agilent/Varian 800 MHz NMR system, using a cryoprobe.

One-dimensional versions of the standard ^{15}N R_1 and ^{15}N R_2 HSQC experiments (with cross-correlation, but with without R_{ex} suppression) were carried out (47). In these experiments, amide proton magnetization is transferred to the amide ^{15}N, where it is allowed to decay according to ^{15}N R_1 or R_2 relaxation mechanisms and transferred back to the amide proton for observation. R_2 relaxation is faster for larger than for smaller molecules; R_1 relaxation is slower for larger than for smaller molecules. From the ratio, one may calculate the rotational correlation time. For spherical, rigid proteins, the rotational correlation time is proportional to the molecular weight. The data were processed in NMRpipe and exported in text format using the Pipe2txt.tcl routine. The data were then imported into Microsoft Excel. For each spectrum, the ranges 8.7–9.0 ppm (structured core residues) were integrated, and the data were fit to a single exponential decay curve using in-house written nonlinear least square fit code with jackknife error estimation (48).

Steady-state Kinetic Analysis of HO-1, HO-2, and Variants—The HO enzymatic assay was modified from methods described previously (49, 50). Recent studies establish that catalase enhances the linearity of the membrane-bound HO-1-catalyzed reaction (50). In our soluble system, we found a similar benefit of catalase for both HO-1 and HO-2 and therefore included it in the enzymatic assays. The 200-μl reaction contained 0.1 μM HO, 15 μM heme, 0.35 μM BVR, 0.25 μg/μl BSA, 20 units/μl catalase, and varying concentrations of CPR in reaction buffer (50 mM Tris-HCl, pH 8.0, 50 mM KCl). The reaction was incubated at 37 °C for 2 min and then initiated with the addition of 8 μl of 10 mM NADPH. Activity was monitored using a Shimadzu UV-2600 spectrophotometer by following the increase in bilirubin absorbance at 468 nm. The difference extinction coefficient between heme and bilirubin at 468 nm of 43 mM^{-1} cm^{-1} was used.

Size Exclusion Chromatography—For gel filtration experiments, proteins were dialyzed into buffer containing 50 mM Tris-HCl, pH 7.0, 50 mM KCl. After recovery from the dialysis tubing, samples were prepared with 50 μM of the indicated protein, 150 μM heme, and 150 μM $NADP^+$. Gel filtration was conducted with a Shimadzu HPLC with an LC-10AT pump system using a Shodex KW-803 column (Shodex, Torrance, CA). The column was calibrated using gel filtration standards (Bio-Rad), and the void volume was determined using blue dextran (2000 kDa, Sigma).

Surface Plasmon Resonance with HO and CPR—SPR binding experiments were conducted using a BIAcore 2000 (GE Healthcare) at 25 °C in 50 mM Tris, pH 7.0, 50 mM KCl with 0.005% surfactant p20. HO-1 or HO-2 was immobilized directly to the dextran matrix of a research grade CM5 sensor chip by amine coupling according to the manufacturer's instructions (GE Healthcare). The sensor chip surface was activated with NHS/EDC for 7 min. Immobilized proteins were diluted to 0.001 μg/μl with 10 mM sodium acetate, pH 4.5, and injected over the sensor chip surface. To minimize nonspecific binding and mass transfer, the immobilization levels were kept below 1000 response units. HO-1 and HO-2 were immobilized to 900 and 300 response units, respectively.

For kinetic analysis of CPR and HO, 45 μl of varying concentrations of CPR were injected at a flow rate of 20 μl/min. Chip regeneration was conducted with a 5-μl injection of 0.5 mM NaCl. A blank reference cell was subtracted from the experimental data. To determine kinetic parameters, three independent experiments were initially analyzed using BIAevaluation software (GE Healthcare) and fit to a 1:1 Langmuir binding model or a bivalent analyte model. Because these models fit the data poorly, the association phase of CPR binding to HO was analyzed using single exponential fits (GraphPad 6.0). Kinetic constants were determined from the linear regression of k_{obs} values plotted against CPR concentration.

For experiments with immobilized CPR, human CPR was immobilized to the CM5 chip according to previously described methods for immobilization of rat CPR (24). Briefly, CPR was immobilized via thiol groups of cysteine residues with the coupling reagent 2-(2-pyridinyldithio)ethaneamine). To stabilize the enzyme and protect residues near the NADPH-binding site, NADPH was included during the immobilization of CPR. CPR was immobilized to ~2000 response units. Others have reported that modification of CPR by 2-(2-pyridinyldithio) ethaneamine) does not affect enzyme activity (24). Binding analysis with immobilized CPR was performed identically to those described above, with freshly prepared hemin as the soluble analyte.

Sedimentation Velocity Analysis—Binding interactions between HO-2 and CPR were analyzed by sedimentation velocity experiments using a method described previously (51). Sedimentation velocity experiments were performed on an Optima XL-I analytical ultracentrifuge (Beckman Coulter, Inc.) equipped with an eight-hole An50Ti rotor. Prior to analysis, HO-2 and CPR were dialyzed against 50 mM Tris, pH 8.0, containing 150 mM NaCl. CPR (20.5 μM) was then mixed with increasing concentrations of HO-2 (0–55 μM), and the resulting protein mixtures (400 μl) were loaded into the sample compartment of a

double-sector cell. The reference compartment was filled with 430 μl of the dialysate buffer. Sample cells were then incubated at 20 °C in the rotor chamber for 2 h under vacuum. After 2 h of incubation, samples were sedimented at 40,000 rpm. A total of 180 absorbance scans (450 nm) at 3-min intervals were collected. Absorbance values ranged from 0.2 to 0.8 for the different samples. The data were analyzed by SEDFIT version 10.58d (52) using the continuous *c*(*s*) distribution model and allowing the frictional ratio to float. CPR-/HO-2 interactions were monitored by integrating the *c*(*s*) distribution between 4 and 7 S to determine the weight-average *s* value of the new observed boundary component (51). A K_d value for the CPR·HO-2 complex was estimated by plotting the weight-average *s* value as a function of HO-2 and fitting the data to a single-site binding isotherm.

Chemical Cross-linking—The reducible, heterobifunctional cross-linker (succinimidyl 6-(3-[2-pyridyldithio]-propionamido)hexanoate) (LC-SPDP) was used in a two-step reaction according to the manufacturer's instructions (Thermo Scientific/Pierce). HO-1 or HO-2 was activated as follows. A fresh 3 mM solution of LC-SPDP was prepared in DMSO. 10 μM HO-1 or HO-2 was prepared in conjugation buffer (0.1 M HEPES), pH 7.5, 30 mM EDTA, 150 mM NaCl and incubated with 0.1 mM LC-SPDP for 30 min at room temperature. Unconjugated cross-linker was then removed by three rounds of buffer exchange using 10,000 molecular weight cutoff Amicon microconcentrators (Millipore, Billerica, MA). 10 μM BVR, CPR, or RNase was then added to the activated protein, and the reaction was incubated at 4 °C overnight. Cross-linking reactions were analyzed by 5–15% gradient sodium SDS-PAGE (Bio-Rad) and visualized by staining the gel with Coomassie Blue (53).

Co-purification of BVR with HO-2—For the co-purification of BVR with HO-2, the cross-linking reaction was performed exactly as described above; however, HO-2 contained an N-terminal His_6 tag (hisHO-2) that was absent in the other reactions. By SDS-PAGE, the cross-linked products of the reaction containing hisHO-2 and BVR migrated to identical positions as those in which the His_6 tag had been removed from HO-2. Samples of hisHO-2 alone, BVR alone, or cross-linked hisHO-2/BVR were incubated with 100 μl of Ni-NTA resin (50% slurry) for 2 h at 4 °C. Samples were rotated on a Boekel variable speed mini-tube rotator (Fisher). Affinity resin and associated proteins were harvested by centrifugation for 5 min at a setting of 2400 × *g* at 4 °C with an accuSpin Micro 17R refrigerated microcentrifuge (Fisher) and washed three times with 1 ml of wash buffer (50 mM Tris-HCl, pH 8.0, 30 mM NaCl, 20 mM imidazole). Protein bound to the resin was eluted with 50 mM Tris-HCl, pH 8.0, 30 mM NaCl, 300 mM imidazole. Eluted fractions were boiled for 5 min in SDS-PAGE loading buffer (50 mM Tris-HCl, pH 6.8, 2% (w/v) SDS, 0.1% (w/v) bromphenol blue, 10% (v/v) glycerol, and 100 mM dithiothreitol) and separated by 10% SDS-PAGE (53). Proteins were then transferred to a nitrocellulose membrane and detected using antibodies against either HO-2 (18) or BVR (Abcam, Cambridge, MA).

Modification of BVR with CPM—Human BVR was modified with 7-diethylamino-3-(4′-maleimidylphenyl)-4-methylcoumarin (CPM) according to methods used to modify rat BVR (27). A 20 mM solution of CPM was prepared in dimethyl sulfoxide. 10 μM BVR with 1 mM NADPH was incubated in the dark with 100 μM CPM at 4 °C for 16 h. Free CPM was removed using a PD-10 desalting column (Amersham Biosciences). Labeled BVR was then frozen and stored in the dark at −80 °C. BVR-CPM was analyzed by LC MS/MS to determine the location of the CPM modification.

Fluorescence Resonance Energy Transfer (FRET) Analysis of the Interaction of HO-1 or HO-2 with BVR—FRET experiments to examine HO-1 or HO-2 binding to human BVR were conducted according to previously described methods for rat BVR (27). Briefly, because the UV-visible spectra of heme-bound HO-1 and HO-2 overlap the fluorescence emission spectrum of the fluorescent probe CPM, binding of heme-bound HO should result in fluorescence quenching of BVR-CPM. BVR-CPM (0.05 μM) was titrated with various concentrations of heme-bound HO-1, heme-bound HO-2, or heme, and fluorescence was monitored at 450 nm with excitation at 350 nm. These experiments were performed in 0.1 M potassium phosphate buffer at pH 7.4 on a Shimadzu FR-5301PC spectrofluorophotometer.

Heme Binding BVR by Optical Absorbance—To obtain the absorbance spectrum of heme-BVR, the difference spectra between 350 and 700 nm were recorded for 2.5 μM BVR with 2.0 μM heme, whereas the reference cuvette contained 2.5 μM BVR alone. To determine binding affinity of heme for BVR, 10 μM hemin was titrated with increasing amounts of BVR (0.5–5.0 μM) with 10 μM heme alone in the reference cuvette. Absorbance at 415 *versus* BVR concentration was fit to a single site binding model using GraphPad Prism 6.0. To assess the ability of BVR to bind heme from hHO-2, 5 μM of hHO-2 was incubated with varying concentrations of BVR (1.0–20.0 μM), and the absorbance spectra from 250 to 700 nm was collected, with the reference cuvette containing 5 μM hHO-2. hHO-2 was prepared by incubating apoHO-2 with a 5-fold excess of freshly prepared hemin for 1 h at 4 °C. Unbound heme was removed using a PD10 desalting column according to the manufacturer's instructions (GE Healthcare). For all experiments fresh hemin was used and was prepared as described above. All spectra were collected on a Shimadzu UV-2600 spectrophotometer.

RESULTS

Various forms of HO and CPR lacking their transmembrane segments were used in these studies. These are HO-1(1–265) containing residues 1–265, HO-2(1–288), and CPR(66–680). For clarity, these proteins will be referred to simply as HO-1, HO-2, or CPR. In experiments that use heme-bound HO, we refer to the protein as hHO-1 or hHO-2.

NMR Analysis of the Interaction between hHO-2 and CPR—NMR is a highly sensitive method to probe protein/protein interactions. Binding of an NMR-silent protein to an NMR-visible protein can perturb the spectrum in several ways; it can change the chemical shift, alter the line width of a resonance, or affect both chemical shift and line width. If resonances within the NMR spectrum have been assigned, these spectral changes can provide residue-specific information regarding the interface between the two proteins.

We recently assigned 70% of the backbone chemical shifts of the hHO-2 (heme-bound) NMR spectrum by three-dimen-

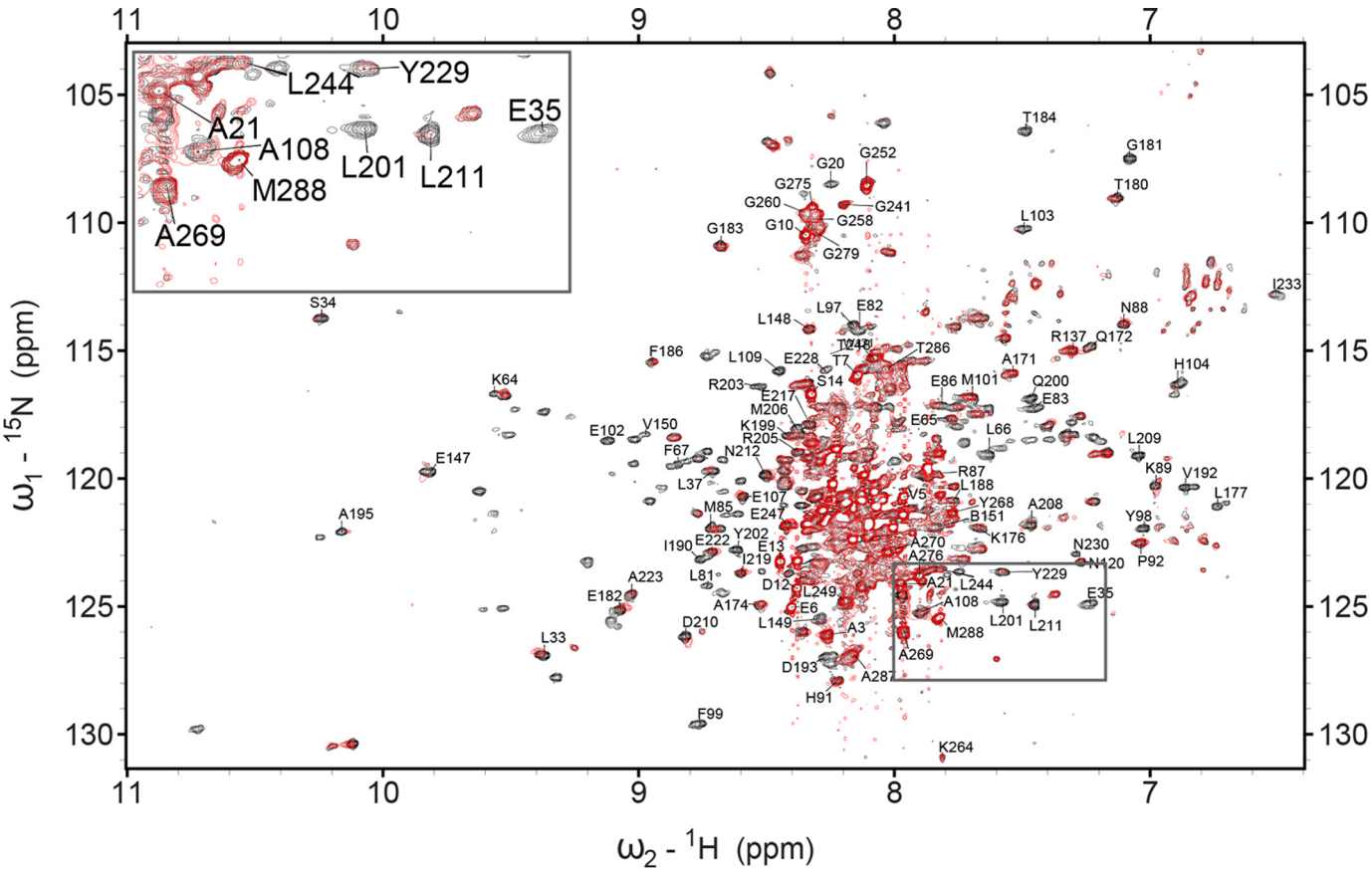

FIGURE 2. **NMR analysis of CPR binding hHO-2.** ^{1}H-^{15}N TROSY spectra of 150 μM perdeuterated ^{15}N-hHO-2 collected in the absence (*black*) or presence (*red*) of equimolar CPR.

sional NMR experiments using a highly concentrated sample (1 mM).[5] To avoid potential nonspecific interaction effects that could arise with highly concentrated protein, in the binding studies described here, we used 150 μM ^{15}N hHO-2 samples. Because large proteins such as HO-2 (~33 kDa) tend to exhibit faster transverse relaxation that reduces signal intensity of the NMR spectrum, we utilized transverse relaxation-optimized spectroscopy (TROSY). TROSY is a method that reduces the ^{1}H and ^{15}N resonance line widths to enhance the spectra of larger proteins (>30 kDa) (54). By applying TROSY, we observe 211 cross-peaks in the ^{1}H-^{15}N TROSY spectrum of perdeuterated ^{15}N-hHO-2, which accounts for resonances arising from ~70% of the hHO-2 residues (Fig. 2). The hHO-2 spectrum consists of resonances arising from both ordered and disordered regions of the protein. Amide proton resonances arising from disordered regions of HO-2 occur in the 7.7–8.6 ppm range, which has a high density of overlapping peaks characteristic of poorly structured regions (46). This region of the spectrum corresponds to the flexible N- and C-terminal domains of hHO-2 residues 1–28 and 243–288. The well dispersed peaks outside of the disordered region arise from the core of hHO-2, as highlighted by the annotated spectra (Fig. 2).[5] Also, in the crystal structure of HO-2 (PDB 2QPP), only the catalytic core of the protein (residues 29–242) is visible, and both the N and C termini are not observed, further supporting the flexibility of the N and C termini (55).

To probe the interface between hHO-2 and CPR, we collected the spectrum of perdeuterated ^{15}N-hHO-2 in the presence or absence of natural abundance CPR (lacking any label). As noted above, we used a lower concentration of hHO-2 (150 μM) than was used earlier to make the assignments to minimize the potential for nonspecific effects such as aggregation. We overlaid the assigned HO-2 spectrum with that collected in the binding studies to determine assignments for the spectrum in the binding studies. Using this method, ~50% of the 288 HO-2 residues in the binding study could be assigned. Analysis of the HO-2 spectrum described below will focus on the assigned region of the protein.

We measured the chemical shift and peak height for resonances in the hHO-2 TROSY spectrum in the presence and absence of CPR. To identify hHO-2 residues that are affected by CPR, we compared the ^{1}H-^{15}N TROSY spectrum of hHO-2 in the presence of equimolar unlabeled CPR with that of hHO-2 alone. The addition of CPR to hHO-2 causes changes in hHO-2 chemical shifts and also decreases in peak intensities for a number of hHO-2 residues (Fig. 2). This peak intensity loss is consistent with an increase in molecular weight and concomitant reduction of TROSY intensity that we would expect to occur as hHO-2 molecular weight increases with the binding of a 70-kDa protein such as CPR (46, 56).

[5] I. Bagai, S. W. Ragsdale, and E. R. P. Zuiderweg, manuscript in preparation.

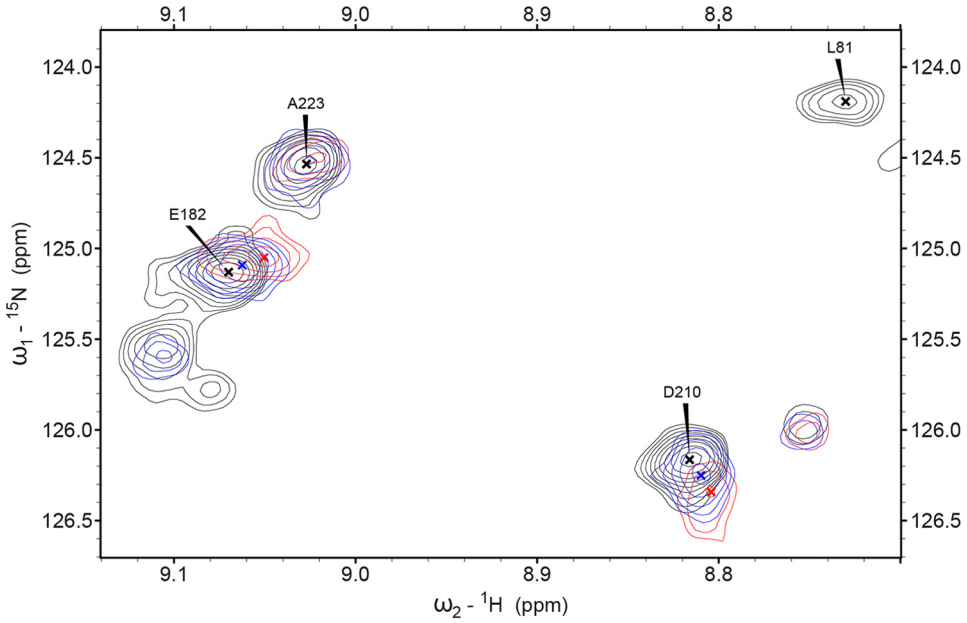

FIGURE 3. **Effect of CPR on hHO-2 chemical shifts.** Detail of the ^{1}H-^{15}N hHO-2 spectrum with 0, 75, or 150 μM CPR (*black*, *blue*, and *red*, respectively) highlighting cross-peaks that experience significant perturbations of the chemical shift or significant intensity loss. Glu-182 and Asp-210 show highly significant change in chemical shifts, although Leu-81 is broadened beyond detection with the addition of CPR. *x* represents the center of the indicated cross-peak. Highly significant changes in CSP are greater than two standard deviations from the mean CSP for assigned residues.

The addition of CPR to hHO-2 also results in CSPs for some hHO-2 cross-peaks (Fig. 3). This demonstrates that the kinetics of binding is in the fast or intermediate fast exchange for which the resonance position ω_i^{obs} of a certain residue i is given by Equation 1 (57),

$$\omega_i^{obs} = f_{free}\omega_i^{free} + f_{bound}\omega_i^{bound} \quad \text{(Eq. 1)}$$

where f_{free} and f_{bound} are the molar fractions of free and complexed HO-2, and where ω_i^{free} and ω_i^{bound} are the chemical shifts in radians of that resonance in those states. Equation 1 holds for both ^{1}H and ^{15}N dimensions in the TROSY spectrum.

To quantify CSPs, the ^{1}H and ^{15}N chemical shift difference was calculated by comparing the chemical shifts of hHO-2 alone with those of CPR. The combined ^{15}N/NH chemical shift change was calculated as the chemical shift change vector as described under "Experimental Procedures." Of the 47 assigned cross-peaks in the N and C termini, none exhibit significant CSPs with the addition of equimolar CPR; however, 28 residues from the HO-2 core exhibit significant CSPs (Fig. 4). Mapping the residues with significant CSPs onto the hHO-2 crystal structure highlights contiguous patches of residues on HO-2 that are likely involved in binding CPR or experience allosteric effects upon CPR binding (Fig. 5). Equally important, there are also many assigned resonances that do not shift, and they also form contiguous patches.

For the range $0.1 < f_{free}$ or $f_{bound} < 0.9$, the line width, LW_i^{obs}, for a resonance i in the fast/intermediate exchange regime is given by Equation 2 (57).

$$LW_i^{obs} = f_{free}LW_i^{free} + f_{bound}LW_i^{bound} + f_{free}f_{bound}\frac{(\omega_i^{free} - \omega_i^{bound})^2}{(1 + f_{bound}/f_{free})k_{off}} \quad \text{(Eq. 2)}$$

Here, the first two terms represent the increase in line width due to a change in the time-averaged molecular weight of HO-2, although the latter term, called exchange broadening, is excess broadening due to the kinetics of binding.

The increase in line width causes a loss in TROSY cross-peak height by two processes as follows: the first is a linear effect and occurs because a broader line in the spectrum has a lower peak height; the second is a strongly nonlinear effect due to a decrease in the coherence transfer efficiencies in the TROSY experiment itself. For large proteins that bind to other large proteins, the second effect is dominant.

To quantify the peak intensity loss in the hHO-2 spectrum upon CPR binding, the peak intensity ratio was determined by dividing the cross-peak intensity in the presence of CPR by the cross-peak intensity from the hHO-2 alone spectrum (+*CPR*/−*CPR*, Fig. 6). A ratio of 1 indicates no effect, although a decreased ratio indicates line broadening for that resonance. Cross-peaks derived from residues located at the HO-2 N and C termini (residues 1–28 and 243–288) are largely unaffected by the addition of equimolar CPR; of the 47 assigned cross-peaks, only four exhibit chemical shift intensity ratios of less than 0.8 (Gly-20, Ala-245, and Glu-247). This is in contrast to the 96 assigned cross-peaks located at the core of HO-2 (residues 29–242); 88 resonances exhibit an intensity ratio of less than 0.8, and 23 have disappeared likely due to broadening beyond detection (Fig. 6). Mapping the intensity ratios onto the hHO-2 crystal structure shows the residues that are most strongly affected by CPR are on the heme binding face of hHO-2 (in which the heme binding pocket and surrounding residues are visible), although residues on the opposite face (180° rotation) of hHO-2 are less affected (Fig. 7).

The interaction areas determined from intensity changes (Fig. 5) and chemical shift changes (Fig. 7) do overlap in general,

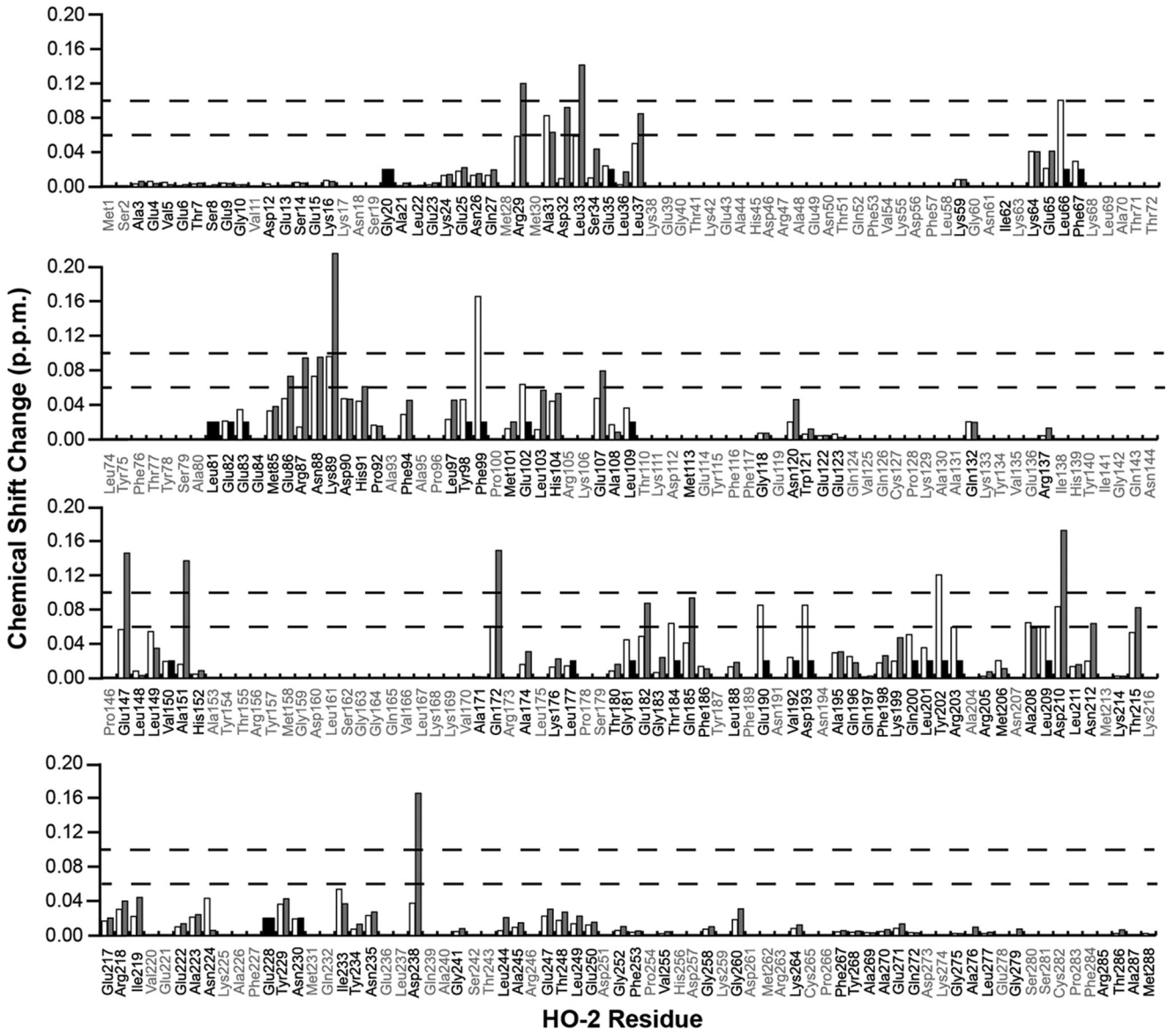

FIGURE 4. **Effect of CPR on hHO-2 chemical shifts.** *Histogram bars* represent the combined ^{15}N/NH chemical shift perturbation (*CSP*) for assigned residues in the hHO-2 spectrum in the presence of 75 or 150 μM CPR (*white* or *gray*, respectively). The CSP for the assigned cross-peaks, measured between the 0 μM CPR spectrum and the 75 or 150 μM CPR spectrum, was calculated from the square root of the sum of the squared N^{1}H and ^{15}N CSPs. Cross-peaks that have broadened beyond detection with the addition of CPR are shown as *black bars* of uniform height. *Dotted lines* indicate CSPs that are significant (1 standard deviation from the mean) or very significant (2 standard deviations from the mean). *Bars* with *gray labels* represent resonances that are unassigned, and assigned residues are in *black*.

suggesting the main binding area is identified by both observables. However, the intensity changes and chemical shifts do not correlate per residue. The most compelling case occurs for the resonance of Leu-201, which completely disappears although it does not shift. As discussed below, this discrepancy indicates a complex binding mechanism.

Titration of CPR into hHO-2 by NMR—If the effects of CPR on the hHO-2 spectrum are due to CPR binding, changes induced by CPR should be titratable. Thus, additional experiments were conducted with 50, 150, 200, and 300 μM CPR, and the resonance height ratio was calculated as described above (Figs. 8 and 9). Under these conditions, using hHO-2 that was not perdeuterated, we observed 165 cross-peaks in the ^{1}H-^{15}N hHO-2 spectrum, which accounts for resonances arising from ~60% of the hHO-2 residues. Comparison of these spectra with the assigned spectrum allows for assignment of 36% of 288 HO-2 residues (Fig. 9).

To quantify the effects of CPR on hHO-2 residues, we compared the ^{1}H-^{15}N TROSY spectrum of hHO-2 in the presence of CPR to that of hHO-2 alone. Although the addition of CPR to hHO-2 does not cause observable changes in hHO-2 chemical shifts in the TROSY spectrum for non-perdeuterated hHO-2, a decrease in peak intensity for a number of hHO-2 residues proportional to the concentration of CPR is observed (Fig. 9). Although titratable changes in the HO-2 spectrum could conceivably result from CPR-dependent catalytic activity of HO-2, this is unlikely to be the cause of the observed intensity changes because NADPH is not present in the NMR experiment and HO-2 is inactive in its absence. Furthermore, CPR causes similar peak height reduction for the apoHO-2 spectrum, here sub-

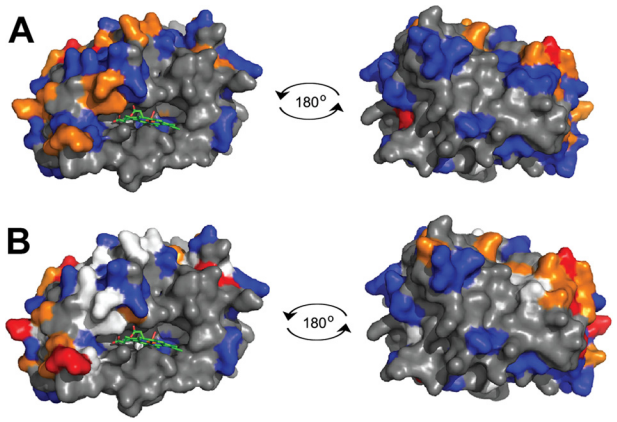

FIGURE 5. **CPR-induced CSPs on the hHO-2 spectrum mapped onto the crystal structure.** The effect of 75 or 150 μM CPR (*A* and *B*, respectively) on hHO-2 CSPs as determined in Fig. 4 was mapped onto the crystal structure of hHO-2 (PDB 2QPP). The color of the residue reflects the degree of CSP effect by CPR. *Red* indicates residues with highly significant CSPs (more than two standard deviations from the mean); *orange* indicates residues with significant CSPs (at least one standard deviation from the mean); *blue* indicates residues with no significant CSP; *white* indicates residues that are broadened beyond detection; *gray* indicates residues that are unassigned.

strate and reducing equivalents are both absent, preventing any catalytic turnover.

Of the assigned residues in the hHO-2 spectrum, the residue that is most affected by the addition of equimolar concentrations of CPR is Leu-201. Glu-107, Ala-208, Leu-209, Leu-211, and Leu-33 are also strongly affected. Although in our 150 μM NMR sample we do not have consecutive assignments for these residues, in the more concentrated multidimensional experiments used for assigning the hHO-2 spectrum Leu-201, Ala-208, Leu-209, and Leu-211 are part of a consecutively assigned region Glu-190–Asn-212. Leu-33 is part of a consecutively assigned region from Arg-29–Leu-37 and Glu-107 is part of a consecutively assigned region from Glu-107–Leu-109, so the assignments are quite secure.

We also conducted ^{15}N T_2 and T_1 relaxation experiments to estimate the molecular mass of hHO-2 under the NMR conditions. The rotational correlation time of a protein is linearly related to its molecular weight; therefore, ^{15}N spin relaxation rates can be used to determine the molecular weight of a protein in solution (58). The molecular mass estimate for the hHO-2 core was found to be 55 kDa. The mass of monomeric hHO-2(1–288) is 33 kDa and that of the hHO-2 core (29–242) is 25 kDa. Thus, the NMR relaxation experiments indicate that hHO-2 is a dimer under the present conditions (>40 μM protein).

NMR Analysis of the Interaction between apoHO-2 and CPR—To test the ability of CPR to bind apoHO-2, the ^{1}H-^{15}N spectrum of 500 μM non-perdeuterated ^{15}N-apoHO-2 was collected in the presence or absence of 100 μM CPR, as described for hHO-2. The addition of CPR to apoHO-2 causes a loss of intensity for apoHO-2 cross-peaks similar to what is observed in the hHO-2 spectrum (Fig. 10). In the apoHO-2 spectrum, 121 distinct cross-peaks are visible, representing ~40% of HO-2 residues. Although assignments for the apoHO-2 spectrum have not been determined, changes in chemical shift intensity were quantified by calculating the chemical shift height ratio (+CPR/−CPR) for each of the cross-peaks. Of the 121 distinct cross-peaks analyzed in the apoHO-2 spectrum, 19 exhibit a chemical shift height ratio of less than 0.8, indicating a loss of cross-peak height for the corresponding HO-2 residues. Changes in chemical shift are not observed for any cross-peaks in the non-perdeuterated spectra. These data indicate that CPR is capable of binding apoHO-2 as well as hHO-2.

Assignments have not been independently determined for the apoHO-2 TROSY spectrum, and the spectrum is distinct from that of hHO-2 (Fig. 11). However, some isolated cross-peaks of the hHO-2 spectrum have identical chemical shifts as in the apoHO-2 spectrum, allowing for a reasonable assignment of the apoHO-2 cross-peak from the hHO-2 spectrum, notably Leu-201 (Fig. 11). Strikingly, of the 121 cross-peaks analyzed, the cross-peak at the location of Leu-201 in the apoHO-2 spectrum is the most sensitive to the addition of CPR, similar to what was observed for the hHO-2 spectrum.

Steady-state Kinetic Analysis of HO-1 and HO-2 Mutants—Residues that exhibit large changes in the hHO-2 NMR spectrum upon binding CPR could be present at the interface of HO-2 and CPR, or alternatively, they could change their chemical environment due to long range conformational changes in HO-2 induced by CPR binding at a distant site. Based on the hypothesis that mutation of residues at the HO-2/CPR interface would lead to an increase in K_d values for the HO-2·CPR complex and, thus, an increased K_m value for CPR, we tested the effect of alanine substitutions on steady-state kinetic parameters for Leu-201 and Lys-169, which were expected to exhibit higher K_m values, and Arg-87, which was used as a control. If a residue exhibits changes in the NMR spectrum by indirect effects (*e.g.* due to a conformational change), making a conservative mutation of that residue is unlikely to affect the K_d or K_m values. Also, we note that HO-2 is likely a homodimer in the NMR binding studies. If a resonance is affected by a change in HO-2 dimerization state, a mutation of that residue would be unlikely to affect the kinetic parameters of HO-2 and CPR.

Alanine substitution of the HO-2 residue with the cross-peak intensity that is most strongly affected by equimolar CPR in the non-perdeuterated NMR binding studies (Fig. 9), L201A, results in a 3-fold increase in the K_m for CPR and no change in k_{cat} compared with wild type protein (Fig. 12*B* and Table 1). However, the R87A variant of HO-2, whose NMR cross-peak height is not strongly affected by the addition of CPR, exhibits no change in the k_{cat} or K_m values for CPR (Fig. 12*B* and Table 1). These results are consistent with a role for Leu-201 at the binding interface for CPR.

We also studied the K169A variant of HO-2 because alanine substitution of Lys-149, the analogous residue in HO-1, exhibits a 7–10-fold increase in the K_d value of the HO-1·CPR complex (24, 27). We observe an ~20-fold increase in the K_m value of the K169A variant of HO-2 for CPR (Fig. 12*B*, Table 1) and a 40-fold increase in the K_m value for the K149A variant of HO-1 (Fig. 12*A* and Table 1). These results indicate that this lysine residue of HO-2 and HO-1 is involved in binding CPR.

Gel Filtration Analysis of the Binding of hHO-1, hHO-2, and CPR—In an attempt to observe the complex between CPR and HO-2 (and HO-1) by other methods, we performed gel filtration experiments. K_d values ranging from ~0.5 to 2.0 μM have been reported for hHO-1 and CPR, and NADP$^+$ is reported to

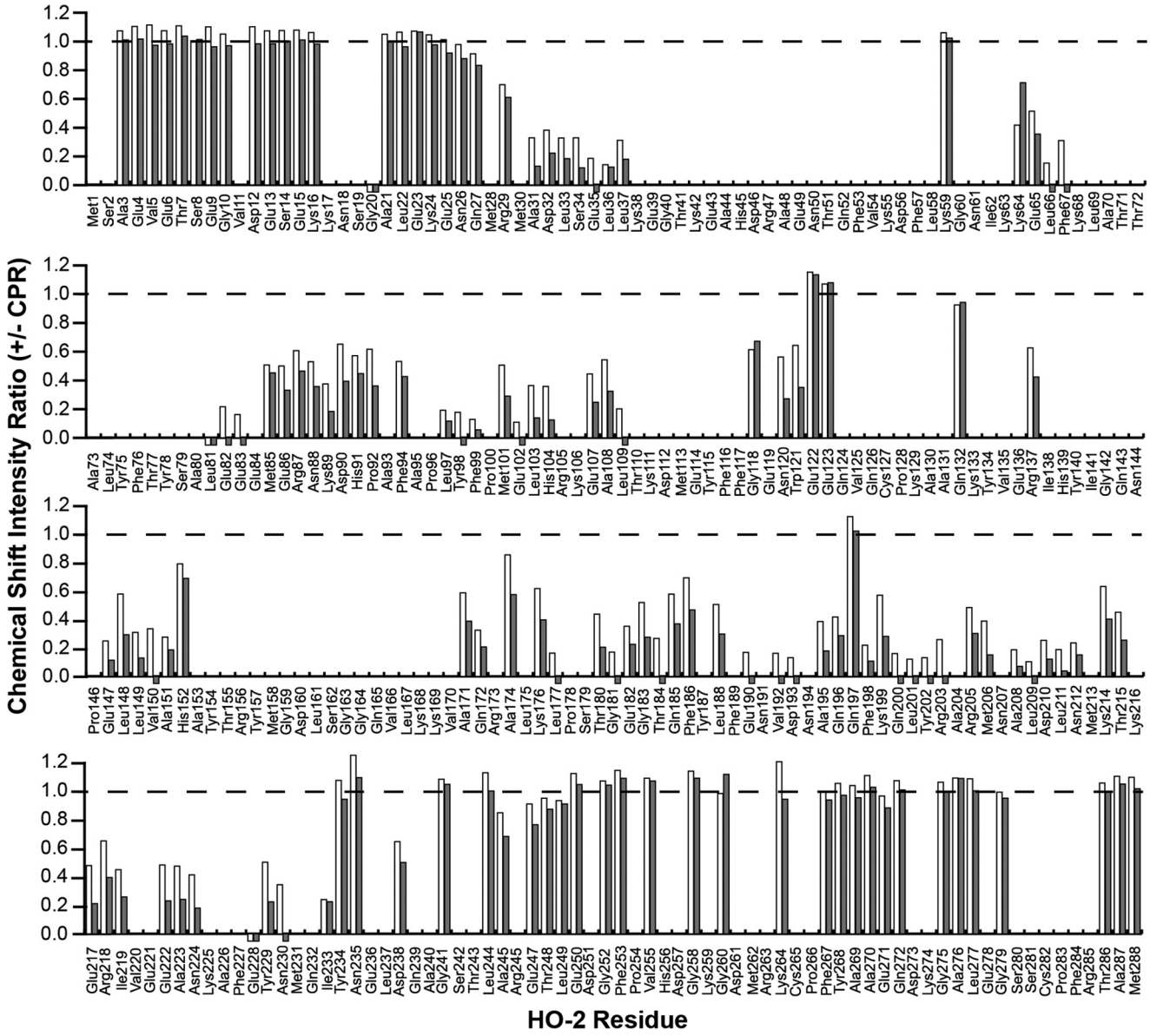

FIGURE 6. **Effect of CPR on perdeuterated hHO-2 chemical shift intensities.** *Histogram bars* represent the ratio of peak height in the absence or presence of CPR (+*CPR*/−*CPR*). Ratios with 75 and 150 μM CPR are shown (*white* and *gray*, respectively). A ratio of 1 (*dotted line*) indicates no change for that residue. *Negative bars* represent cross-peaks that are broadened beyond detection with the addition of CPR. *Bars* that are absent represent residues that are unassigned in the spectrum.

enhance binding (24, 27). We performed gel filtration experiments with 50 μM HO-1 or HO-2 and equimolar CPR in the presence of 150 μM $NADP^+$ and 150 μM heme. For comparison, the elution of the individual proteins (HO-1, HO-2, and CPR) in the presence of heme and $NADP^+$ was also determined. Because heme or $NADP^+$ could affect the migration of the individual proteins, they were included in 3-fold excess in all samples.

By gel filtration analyses, we did not observe any evidence for a complex between CPR and either hHO-1 or hHO-2 (Fig. 13 and Table 2). CPR migrates at position 1 (~70 kDa) in the absence (*dashed line*) or presence (*red lines*) of hHO-1 or hHO-2 (Fig. 13). Peak 2, which marks the migration of hHO-2 or hHO-1, corresponds to ~60 and 44 kDa, respectively, and shows up as a shoulder in Fig. 8*A* in the HO-1/CPR sample. Consistent with the NMR relaxation studies, these results suggest that hHO-2 exists as a homodimer under these conditions. The difference in apparent mass between HO-1 and CPR is greater than that between HO-2 and CPR; therefore, peaks 1 and 2 are slightly separated in Fig. 13*A* and are overlapped in Fig. 13*B*. The elution profiles of CPR were unaffected by incubation with either HO-1 or HO-2; for example, a CPR·HO-2 complex, which would have eluted at a position corresponding to ~100 kDa, was not observed. Others have also failed to observe a complex between wild type HO-1 and CPR by gel filtration (26). The HO·CPR complex is undetected under these conditions, suggesting that the complex is weak and/or highly transient, consistent with the NMR and steady-state kinetic studies.

Binding of CPR to HO-1 or HO-2 by Surface Plasmon Resonance (SPR)—We also attempted to quantify CPR binding to HO-1 and HO-2 using SPR, with HO-1 or HO-2 immobilized

on the dextran surface of the SPR chip through amine chemistry (Fig. 14). Representative association and dissociation curves with various concentrations of CPR (1.25–20 μM) are shown in Fig. 14*A*. The SPR sensorgrams show CPR-dependent association and CPR-independent dissociation phases, clearly demonstrating that CPR binds to both HO-1 and HO-2. To avoid potential artifacts, these experiments were performed in the absence of heme because heme itself produced a strong "binding" response (Fig. 14*E*). Use of the apoproteins is justified by our NMR experiments (above) using apoHO-2 and CPR, which clearly demonstrate that CPR can bind both apoHO-2 and hHO-2.

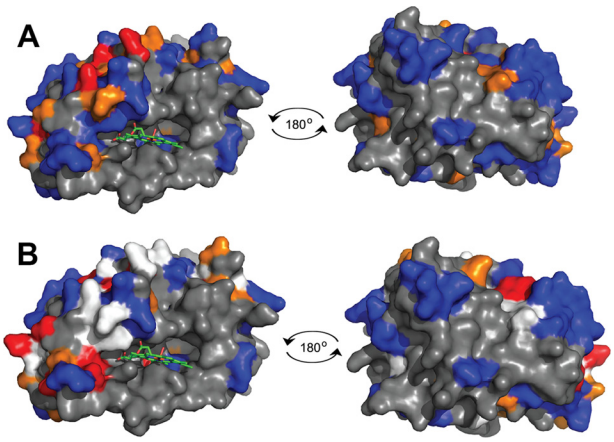

FIGURE 7. **CPR induced changes for hHO-2 cross-peak intensities mapped onto the crystal structure.** The effect of 75 or 150 μM CPR (*A* and *B*, respectively) on hHO-2 cross-peak heights mapped on to the crystal structure of hHO-2 (PDB 2QPP). Cross-peak intensity ratios are as determined in Fig. 6. The color of the residue reflects the degree of effect by CPR. *Red* indicates ratio of $0 < 0.2$; *orange* indicates ratio of $0.2 < 0.3$; *blue* indicates ratio > 0.3; *white* indicates residues that are broadened beyond detection; *gray* indicates residues that are unassigned.

To derive binding kinetic constants from the SPR sensorgrams, the association and dissociation phases were fit individually because simultaneous global fitting analysis of CPR association and dissociation curves using the 1:1 Langmuir model (BIAevaluation) produces a poor fit to the data. Single exponential fits of the association phase (GraphPad Prism6) of CPR and HO-1 or HO-2 were used to determine k_{on} values (0.0010 ± 0.0002 and 0.0014 ± 0.0002 s^{-1} μM^{-1}) and k_{off} values (0.020 ± 0.003 and 0.0230 ± 0.0003 s^{-1}) for CPR binding to HO-1 or HO-2, respectively (Fig. 14, *B* and *C*). From these k_{on} and k_{off} values, the K_d values of 20.5 ± 7.6 and 16.7 ± 2.5 μM were determined for CPR and HO-1 or HO-2, respectively, indicating that these proteins form relatively weak (transient) complexes. Biexponential fits of the dissociation curves (Fig. 14*D*) indicate a fast and slow dissociation phase, with k_{fast} values in reasonable agreement with the values determined by linear regression analysis of the binding data ($k_{fast} = 0.026 \pm 0.002$ and 0.035 ± 0.008 s^{-1}; $k_{slow} = 0.0030 \pm 0.0015$ and 0.0025 ± 0.0005 s^{-1} for HO-1 and HO-2, respectively).

Sedimentation Velocity Analysis of HO-2 and CPR—Binding interactions between CPR and HO-2 were also analyzed by sedimentation velocity ultracentrifugation, a method that is less sensitive to heme artifacts than SPR. As described under "Experimental Procedures," 20.5 μM CPR was titrated with varying concentrations of heme-bound HO-2 (0–55 μM). In these experiments, the sedimentation coefficient distribution of CPR was monitored in the presence of increasing concentrations of hHO-2. Fig. 15*A* shows a sedimentation velocity profile obtained with a 2:1 molar ratio of hHO-2 to CPR. In the absence

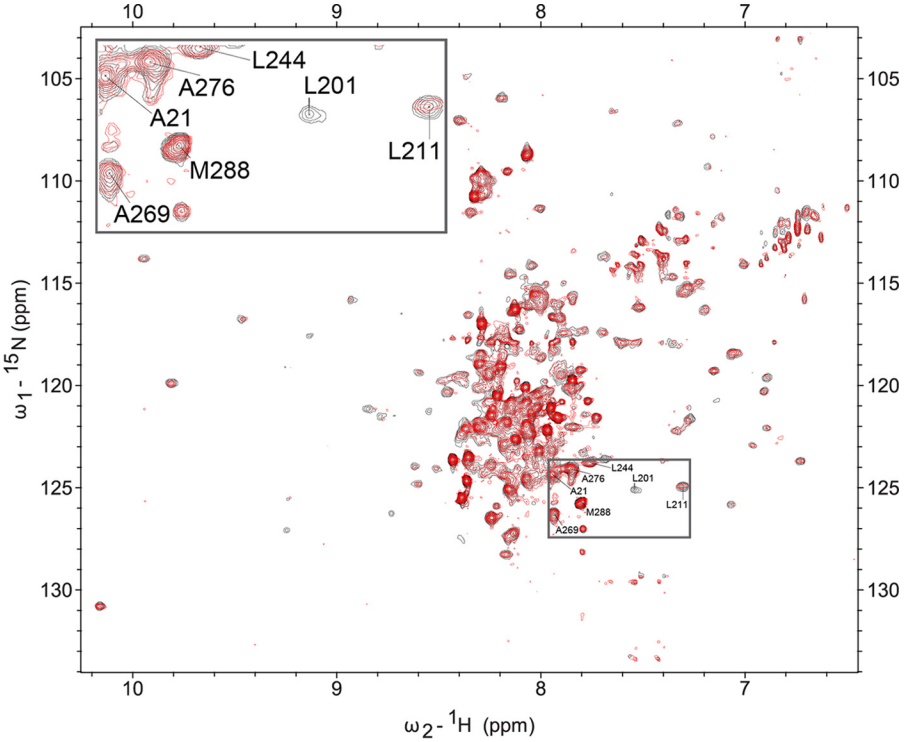

FIGURE 8. **NMR analysis of CPR binding non-perdeuterated ^{15}N hHO-2.** ^{1}H-^{15}N TROSY spectra of 150 μM non-perdeuterated ^{15}N-hHO-2 collected in the absence (*black*) or presence (*red*) of equimolar CPR.

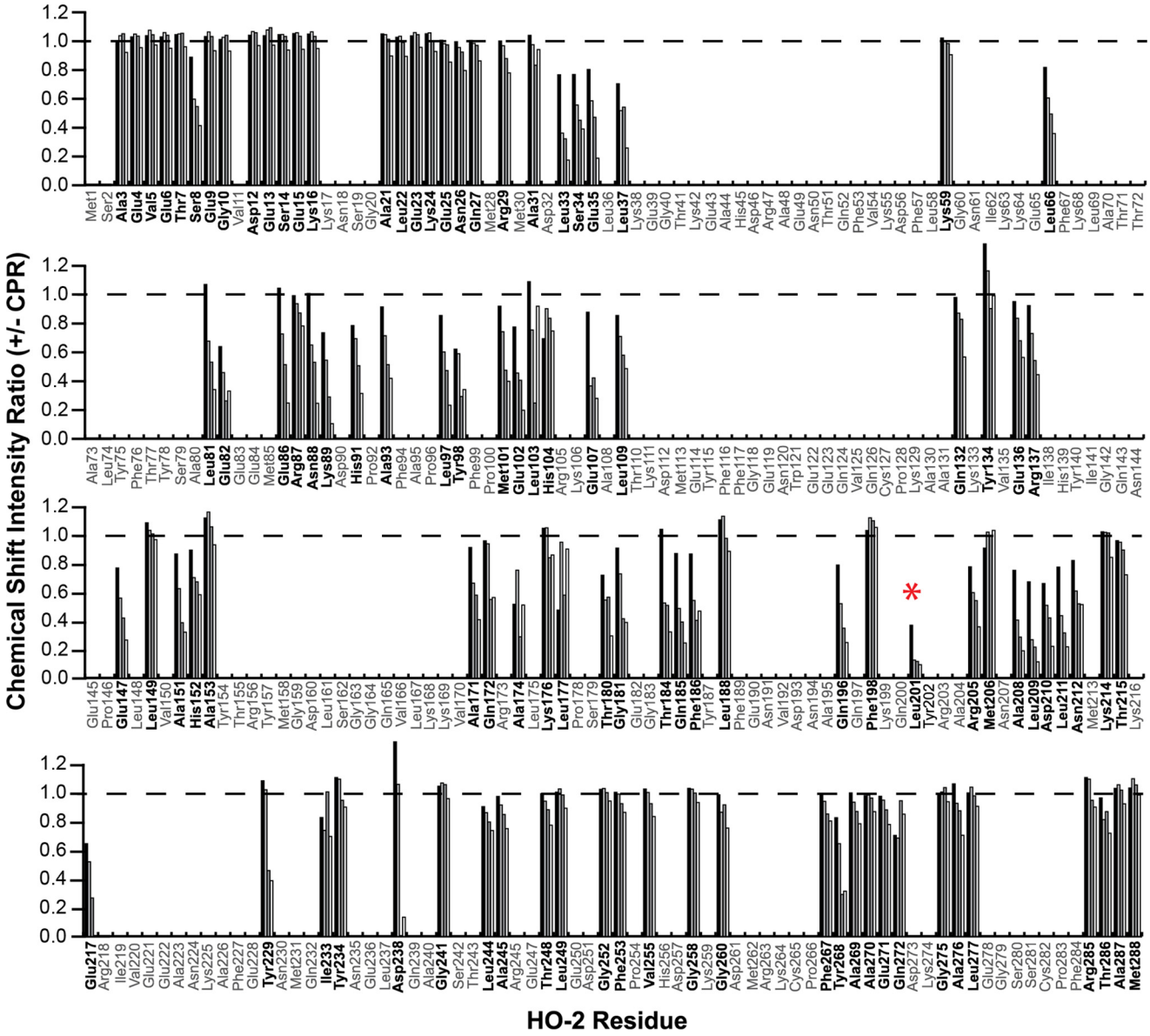

FIGURE 9. **Effect of various concentrations of CPR on non-perdeuterated ^{15}N-hHO-2 resonances.** *Histogram bars* represent the ratio of resonance height in the absence or presence of CPR (*+CPR/−CPR*). Ratios with 50, 150, 200, and 300 μM CPR are shown (*black, light gray, dark gray,* and *white bars,* respectively). A ratio of 1 (*dotted line*) indicates no change for that residue. *Bars* that are absent (*gray labels*) represent resonances that are unassigned, and assigned residues are in *bold*. The *asterisk* highlights Leu-201 as the cross-peak that is most sensitive to the addition of CPR.

of hHO-2, CPR is characterized by a sedimentation coefficient centered at 4.5 S as shown in Fig. 15*B*. hHO-2 alone shows two sedimentation coefficients with a major component (60%) centered at 2.8 S and a minor component (34%) at 4.2 S. Upon adding hHO-2, the shape of the CPR component changes with the boundary shifting to a higher sedimentation coefficient. The weight-average *s* value of this fast boundary component was determined by integrating the *c*(*s*) distribution between 4 and 7 S. From these data, a K_d of 15.1 ± 6.5 μM was determined for hHO-2 and CPR. At the highest hHO-2 concentration, the CPR·HO-2 complex was characterized by a weight-average *s* value of 5.2 S.

Chemical Cross-linking of CPR and HO-1 or HO-2—We conducted chemical cross-linking experiments to trap the complex between HO-2 and CPR. Because cross-linking is an irreversible reaction, even transient complexes can be detected. Because CPR has been reported to bind HO-1 (24–27), we used HO-1 and CPR as a positive control. According to the crystal structure (PDB 3QE2), human CPR possesses at least two surface cysteine residues, which should be available for cross-linking. Thus, we utilized the heterobifunctional cross-linker LC-SPDP, which contains both an amine and a thiol-reactive group. As described under "Experimental Procedures," after activating HO-1 or HO-2 and removing unreacted cross-linker, CPR was added, and the reaction was incubated overnight at 4 °C. Stable complexes between CPR and HO-1 as well as CPR and HO-2 were formed (Fig. 16*A*). A small amount of HO-2 homodimer is visible in the HO-2 sample that lacks CPR, although, for activated HO-1 alone, no homodimeric complex was observed.

As a negative control, we activated the HOs as described above and incubated with a physiologically unrelated cysteine-containing protein, RNase, instead of CPR. RNase (based on

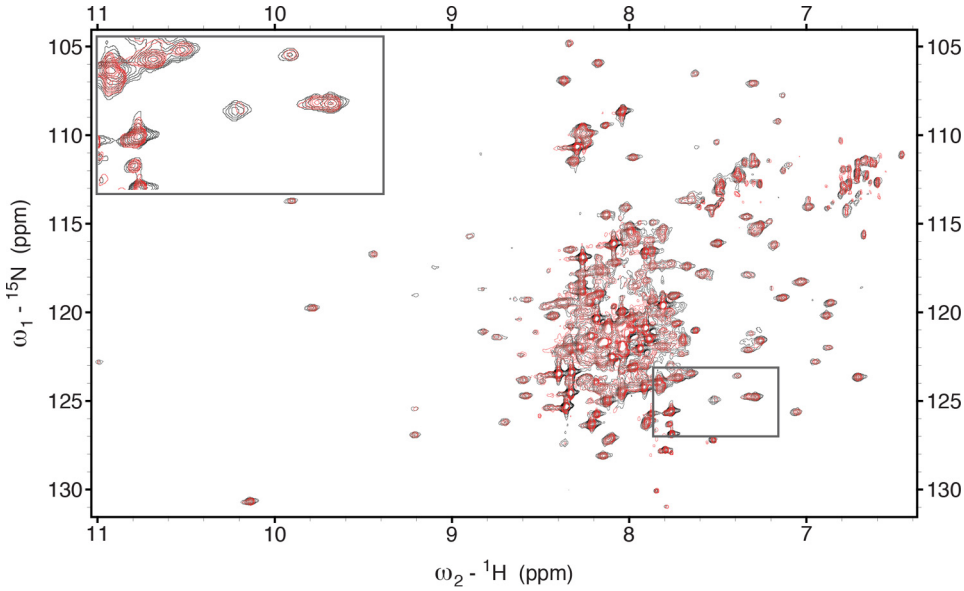

FIGURE 10. **NMR analysis of CPR binding apoHO-2.** ^{1}H-^{15}N TROSY spectra of 500 μM non-perdeuterated ^{15}N-apoHO-2 collected in the absence (*black*) or presence (*red*) of 100 μM CPR.

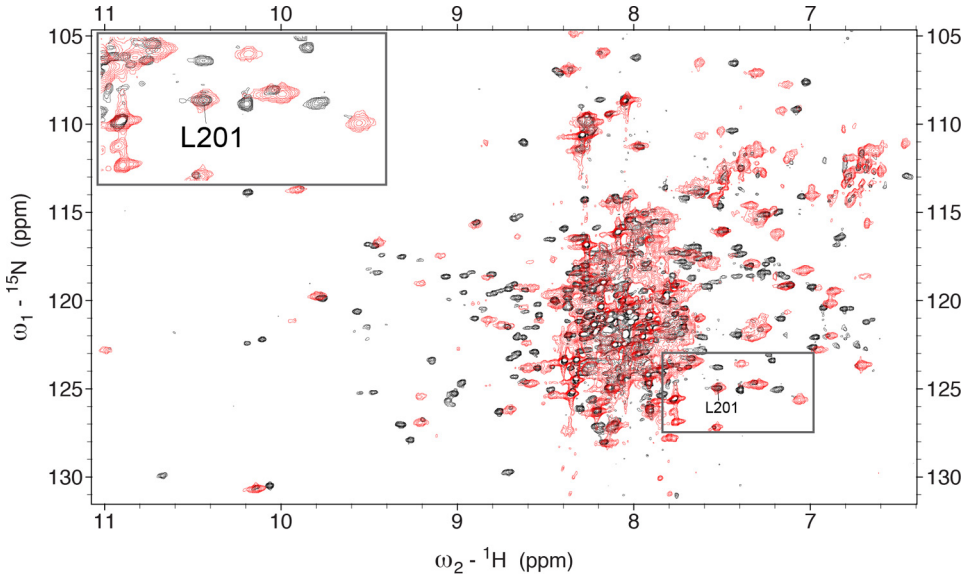

FIGURE 11. **TROSY spectra of hHO-2 (*black*) and apoHO-2 (*red*).** ^{1}H-^{15}N TROSY spectra of 150 μM non-perdeuterated ^{15}N-hHO-2 (*black*) or 500 μM non-perdeuterated apoHO-2 (*red*). The cross-peak assigned as Leu-201 for the hHO-2 spectrum is identified.

PDB 1RCA) contains eight cysteine residues, four of which are surface-exposed. No high molecular weight complex between RNase A and either HO-1 or HO-2 was observed (Fig. 16*B*).

NMR Studies of HO-2 in the Presence of BVR—BVR mediates the second step in heme degradation, the conversion of biliverdin to bilirubin. HO-1 and BVR are reported to form a complex with a K_d of 0.2 ± 0.1 μM (24, 27). An overlapping binding site on HO-1 for CPR and BVR has been proposed but with the binding sites not identical (24, 25, 27). To our knowledge, binding of HO-2 and BVR has not been addressed.

To attempt to characterize the binding interface between HO-2 and BVR, we performed NMR experiments similar to those described for HO-2 and CPR. The ^{1}H-^{15}N TROSY spectrum of 150 μM non-perdeuterated ^{15}N-hHO-2 was collected in the absence or presence of equimolar BVR (not labeled with ^{15}N). Although CPR induced obvious changes in the hHO-2 spectrum (Fig. 8), the spectrum of hHO-2 collected in the presence of BVR is almost identical to that of hHO-2 alone (Fig. 17). No changes in the chemical shifts are apparent, and the majority of assigned resonances exhibit a height ratio (+BVR/−BVR) close to 1, indicating no change (Fig. 18). These results suggest that under the NMR conditions (150 μM), BVR binds hHO-2 very weakly, if at all. Experiments with ^{15}N-apoHO-2 and equimolar BVR also showed BVR has no effect on the apoHO-2 spectrum (data not shown).

Our NMR binding studies thus suggest that BVR has a significantly lower affinity for HO-2 compared with CPR. In contrast, others have reported nanomolar K_d values for the BVR·hHO-1 complex (27). Because HO-1 and HO-2 are highly homologous, our results were unexpected. Thus, other experi-

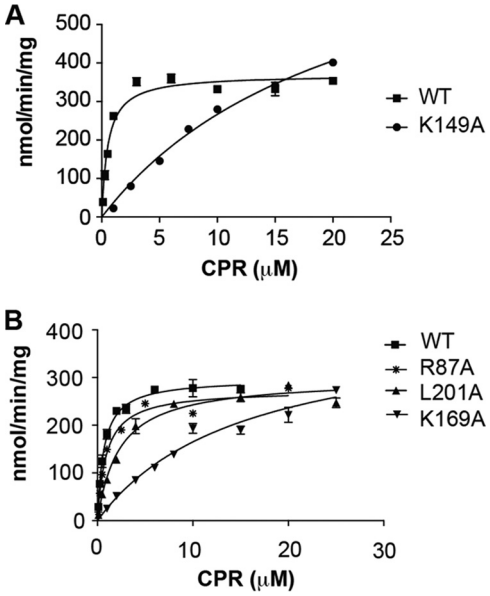

FIGURE 12. **HO mutants have an increased K_m values for CPR.** Heme oxygenase activity for HO-1 (*A*) or HO-2 (*B*) and their respective mutants with varying amounts of CPR. Activity was monitored by observing the formation of bilirubin at 468 nm, as described under "Experimental Procedures."

TABLE 1

Michaelis parameters for HO variants and CPR

Heme oxygenase activity was monitored for HO-1 or HO-2 and the indicated mutants with varying amounts of CPR as shown in Fig. 12. Specific activity is represented as nanomoles of bilirubin/min/mg of HO.

Construct	V_{max}	K_m	K_m
	nmol min^{-1} mg^{-1}	*μM*	*-fold change*
HO-1			
WT	370 ± 12	0.5 ± 0.1	1
K149A	847 ± 64	21.7 ± 2.6	42.4
HO-2			
WT	296.9 ± 4.6	0.7 ± 0.1	1
R87A	275 ± 11	0.9 ± 0.1	1.3
L201A	298.2 ± 8.0	2.3 ± 0.2	3.3
K169A	417 ± 37	15.2 ± 2.6	21.7

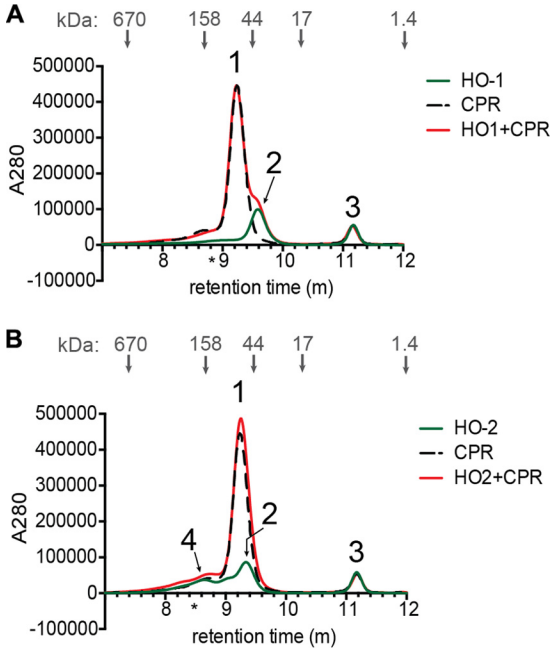

FIGURE 13. **HO and CPR analysis by size exclusion chromatography.** 50 μM CPR and HO-1 (*A*) or CPR and HO-2 (*B*) were loaded onto a Shodex KW-803 gel filtration column individually or in the indicated mixture in the presence of 150 μM heme and 150 μM $NADP^+$ in running buffer (50 mM Tris, 50 mM KCl, pH 7.0). The *asterisk* represents the retention time for a 100-kDa protein, and *gray arrows* mark the position of the molecular weight standards. *Peak 1,* CPR; *peak 2,* heme oxygenase; *peak 3,* $NADP^+$ and heme; *peak 4,* HO-2 aggregate.

TABLE 2

Apparent molecular weight of HO-1, HO-2, and CPR by gel filtration

V_e/V_0 values for the indicated proteins, blue dextran (V_0), B12, and protein standards (Bio-Rad) were measured, and the apparent masses were determined as described under "Experimental Procedures."

Protein	V_e/V_0	Apparent mass
		Da
HO-1	1.565 ± 0.005	44,000 ± 1600
HO-2	1.525 ± 0.002	60,300 ± 1100
CPR	1.509 ± 0.004	68,600 ± 2000
CPR (with HO-1)	1.507 ± 0.004	69,600 ± 2000
CPR (with HO-2)	1.506 ± 0.002	70,000 ± 1300

ments were performed to assess the interaction between the HOs and BVR.

Fluorescence Quenching Experiments Involving BVR-CPM and HO-1 or HO-2—One possible explanation for the lack of NMR evidence for an HO-2/BVR interaction is that HO-2 interacts differently with BVR compared with HO-1. To address this possibility, we repeated the published fluorescence quenching experiments for measuring interactions between HO-1 and BVR (27), and we performed similar experiments to determine the binding affinity of HO-2 for BVR. In these studies, BVR was labeled with the thiol-reactive dye CPM to produce fluorescent BVR upon excitation at 350 nm. Because the hHO-1 absorption spectrum overlaps with the emission spectrum of BVR-CPM, hHO-1 binding results in fluorescence quenching due to FRET processes. Because apoHO has no absorbance in the 350 nm region, this method can only be used to evaluate hHO binding. Plotting the % fluorescence quenching at 455 nm *versus* hHO-1 concentration produced a binding curve (Fig. 19*A*) that fits to a one-site binding model with a K_d of 0.25 ± 0.09 μM, almost identical to the previously reported value of 0.22 ± 0.09 μM (27). Similar FRET experiments with hHO-2 and BVR (Fig. 19*B*) provided concentration-dependent, saturable binding curves with a K_d of 0.27 ± 0.01 μM.

These results suggest that BVR binds both HO-1 and HO-2 with similar high affinity. Equation 3 can be used to estimate a K_d value in situations where the concentration of free ligand cannot be estimated due to high affinity and near stoichiometric binding. If HO-2 and BVR have a K_d of ~300 nM (as suggested by the fluorescence quenching results), Equation 3 predicts 70% of HO-2 should be complexed with BVR under the NMR conditions (with 150 μM HO-2 and 150 μM BVR). This is clearly inconsistent with the NMR results; therefore, we conducted additional experiments to interrogate the source of this apparent discrepancy between the NMR and FRET experiments.

$$EL = 0.5(E_0 + L_0 + K_d - ((E_0 + L_0 + K_d)^2 - 4E_0 \cdot L_0)^{1/2}) \quad \text{(Eq. 3)}$$

Fluorescence Quenching of BVR-CPM by Heme—To attempt to resolve the inconsistency between the NMR and fluores-

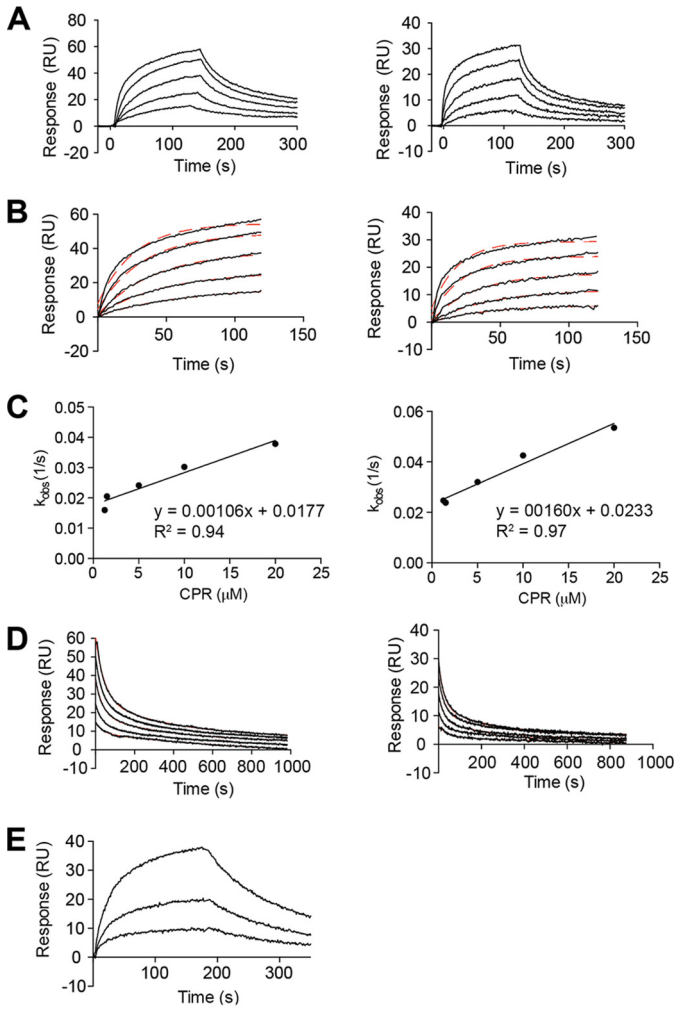

FIGURE 14. **SPR analysis of CPR biding HO-1 (*left panels*) and HO-2 (*right panels*).** *A,* various concentrations of CPR (1.25, 2.5, 5.0, 10.0, and 20.0 μM) were injected against immobilized HO-1 or HO-2. *B,* single exponential fits for the association phase of CPR binding HO-1 or HO-2 are shown in *red*. *C,* single exponential fits were used to determine k_{obs} for the association phase of CPR binding HO-1 or HO-2. k_{on} and k_{off} values are derived from the linear regression of k_{obs} (k_{on} = slope; k_{off} = *y* intercept). *D,* biexponential fits for the dissociation phase of CPR binding HO-1 or HO-2 are shown in *red*. *E,* various concentrations of heme (0.125, 0.25, and 0.5 μM) were injected against immobilized CPR. Data are representative of three independent experiments.

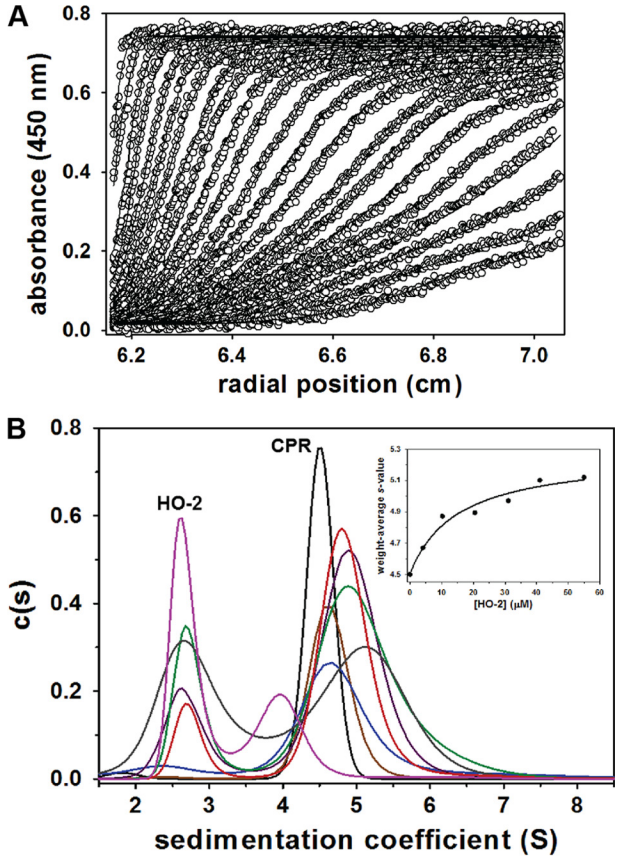

FIGURE 15. **Sedimentation velocity analysis of HO-2 and CPR interactions.** *A,* velocity scans selected from analysis of a 2:1 ratio of hHO-2 (41 μM) to CPR (20.5 μM). Shown are the absorbance data (*open circles*) fitted (*solid lines*) to the continuous *c*(*s*) distribution model. *B,* sedimentation coefficient distributions of CPR (20.5 μM) alone (*black trace*) and in the presence of 4.1 μM (*brown trace*), 10.25 μM (*blue trace*), 20.5 μM (*red trace*), 30.75 μM (*purple trace*), 41 μM (*green trace*), and 55 μM HO-2 (*gray trace*). hHO-2 alone (41 μM) is shown in *magenta*. The *inset* shows the weight-average *s* value plotted *versus* HO-2 concentration. The data were fit to a single-site binding isotherm to yield a K_d value of 15.1 ± 6.5 μM.

cence quenching results, we tested the hypothesis that free heme, dissociating from HO-2, may be responsible for the fluorescence quenching of BVR-CPM. When free heme was titrated into BVR-CPM under conditions identical to those used for hHO titrations, there was strong concentration-dependent and saturable quenching of BVR-CPM fluorescence (Fig. 19*C*), indicating a K_d value of 0.037 ± 0.01 μM. These results suggest that the fluorescence quenching observed in the FRET experiments could be due to the effects of heme binding to BVR, or the CPM fluorophore, rather than the HO protein. Assuming a K_d of 33 nM for HO-2 and heme (17), Equation 3 predicts that 1 μM hHO-2 will contain ~0.17 μM dissociated heme, which is well above the K_d value determined in these experiments. Thus, we suggest that the quenching of BVR-CPM fluorescence observed in the titration with hHO-1 or hHO-2 results from free heme, dissociated from HO, not the HO protein. We propose that the heme binds to BVR-CPM from solution and not through direct heme transfer from the heme-HO complex to BVR. In fact, our results demonstrate that these proteins do not form a complex, dispelling the possibility of a protein-to-protein heme transfer.

The effects of free heme on BVR-CPM fluorescence are consistent with the report that heme binds to BVR and to residues 290–296 of the BVR C-terminal peptide (KYCCSRK) (36). Furthermore, when we analyzed BVR-CPM by LC MS/MS to determine the location of the CPM label, we identified one CPM molecule attached to Cys-204 and another to either Cys-292 or Cys-293 of BVR (Fig. 20). Because Cys-292 and Cys-293 are located on the same peptide in the LC MS/MS analysis, the two cysteines were not distinguished by this analysis.

Although the other surface-exposed Cys (Cys-74) is not observed in this analysis, it is most likely unmodified because BVR-CPM has enzymatic activity similar to that of the wild type protein (109%). We and others (59) find that mutation of Cys-74 in human BVR, or its homolog Cys-73 in rat BVR, ablates enzymatic activity. Additionally, CPM labeling was conducted in the presence of $NADP^+$, which is expected to protect the enzymatic cleft from modification.

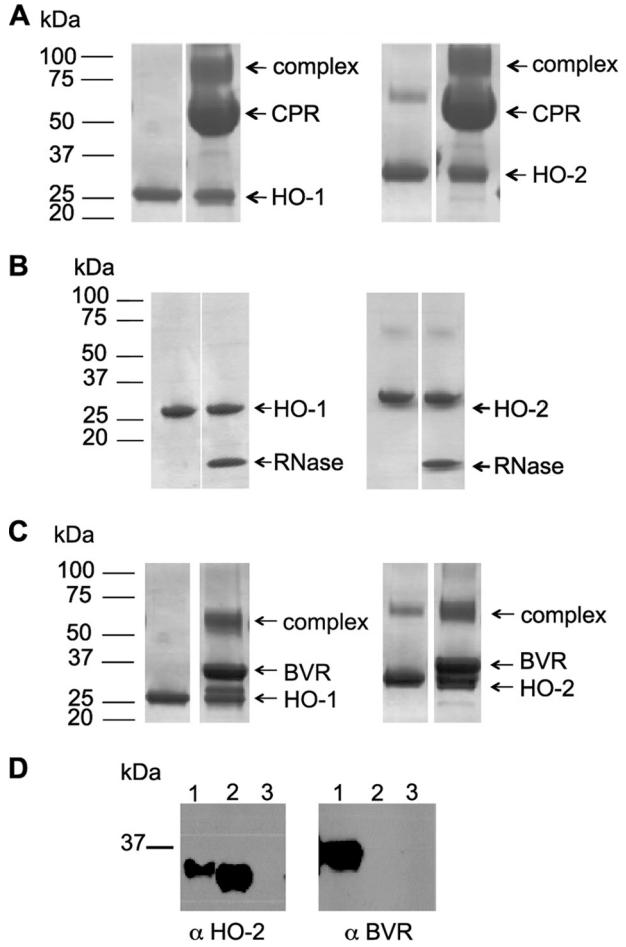

FIGURE 16. **Chemical cross-linking of HO-2 and CPR.** *A,* heterobifunctional cross-linker LC-SPDP stabilizes a complex between HO-1 or HO-2 and CPR. *B,* no complex is trapped for HO-1 or HO-2 with RNase. *C,* chemical cross-linking also stabilizes a complex between HO-1 or HO-2 and BVR. Cross-linking reactions contained 10 μM of the indicated protein. *D,* reducing SDS-PAGE and Western blot of HO-2 pulldown and associated BVR. *Lane 1,* cross-linking reaction; *lane 2,* HO-2 only; *lane 3,* BVR only.

BVR Binding Heme by Optical Absorbance—To further investigate the possibility that the fluorescence quenching of BVR-CPM by hHO-2 results from the binding of free heme by BVR, we titrated BVR with free heme and measured the absorbance spectrum. As observed by others (36), BVR alone shows no optical absorbance in the 350–700 nm range; however, in the presence of heme, we observe the development of an absorbance band with a wavelength maximum at 415 nm, indicating that free heme binds BVR (Fig. 21*A*). To determine the affinity of heme for BVR, 5 μM heme was titrated with BVR, and the absorbance at 415 nm was measured and fit to a single-site binding model, yielding a K_d of 220 $\pm$ 50 nM (Fig. 21*B*).

Titration of BVR-CPM with hHO-2 produces strong fluorescence quenching; however, because there is no evidence of HO-2/BVR binding by NMR, we hypothesize that heme, not HO, is responsible for a large part of the fluorescence quenching. To test whether heme from hHO-2 can bind BVR, we incubated hHO-2 with BVR. Because the absorbance of hHO-2 is ~10-fold greater than that of heme-bound BVR and because the absorbance spectra overlap, hHO-2 was included in the reference cuvette for these titrations. Under these conditions, with increasing concentrations of BVR titrated into hHO-2, absorbance at 415 nm also increases. This result supports that BVR is capable of binding heme from hHO-2 (Fig. 21*C*).

Chemical Cross-linking of HO-2 and BVR—The above results suggest that HO-2 and BVR either do not interact or that that they form a very weak complex. We incubated HO-2, which had been activated with LC-SPDP and with BVR, as described above for trapping the HO-2·CPR complex. Because HO-1 and BVR have been reported to form a complex (24, 27), we also conducted the experiment with HO-1 as a positive control. Under conditions identical to those used to stabilize the HO-2·CPR complex, a high molecular mass complex of ~60 kDa was observed by SDS-PAGE for BVR and both HO-1 and HO-2 (Fig. 16*C*).

Because HO-2 and BVR are similar in molecular mass, a heterodimer of HO-2 and BVR is not distinguishable from either homodimer by size alone. To determine whether BVR is directly linked to HO-2 in the cross-linked product, we conducted the cross-linking reaction using HO-2 that retained an N-terminal His_6 tag (hisHO-2). The cross-linked products with hisHO-2 were identical to those with HO-2 by SDS-PAGE analysis (data not shown). We then isolated hisHO-2 from the cross-linking reaction using Ni-NTA resin and analyzed the proteins that associated with the affinity resin by reducing SDS-PAGE, which was subjected to Western blotting using antibodies against HO-2 or BVR. Under these conditions, the cross-linker undergoes reduction, allowing the proteins to migrate at their native size. BVR was found to copurify with HO-2 in the cross-linked product (Fig. 16*D*). A control reaction demonstrated that BVR alone did not associate with the affinity resin (Fig. 16*D*). These results demonstrate that an HO-2·BVR complex can be trapped by chemical cross-linking.

To identify the location of the cross-linker in the HO-2·BVR complex, we conducted a tryptic digest followed by LC-MS/MS analysis of the cross-linked product. This analysis identified the HO-2 peptide containing Lys-264 (KCPFYAAEQKD) linked to the BVR peptide containing Cys-292 and Cys-293 of BVR (YCCSR), the same peptide shown earlier to bind heme (36).

DISCUSSION

In the HO reaction, seven electron equivalents from NADPH are transferred to the HO-bound heme via CPR. For rapid and efficient electron transfer, the electron donor (flavin on CPR) and acceptor (heme of HO-2) should be at optimal orientation and distance, implying that an electron transfer complex is formed during the catalytic cycle. One of the issues we have addressed in this paper is the existence and nature of that electron transfer complex. One possibility is that HO and CPR form a stable complex within which multiple electrons transfer from NADPH through the bound flavins (FAD and FMN) on CPR to the HO-bound heme as it undergoes oxygenation and conversion to biliverdin and CO. The other possibility is that HO and CPR encounter each other only transiently and associate/dissociate multiple times during each catalytic cycle. Similarly, either HO or BVR forms a stable complex, within which biliverdin is transferred (perhaps channeled) between the two proteins or, as another alternative, remains completely unattached as the HO product (biliverdin) is released into solution and captured

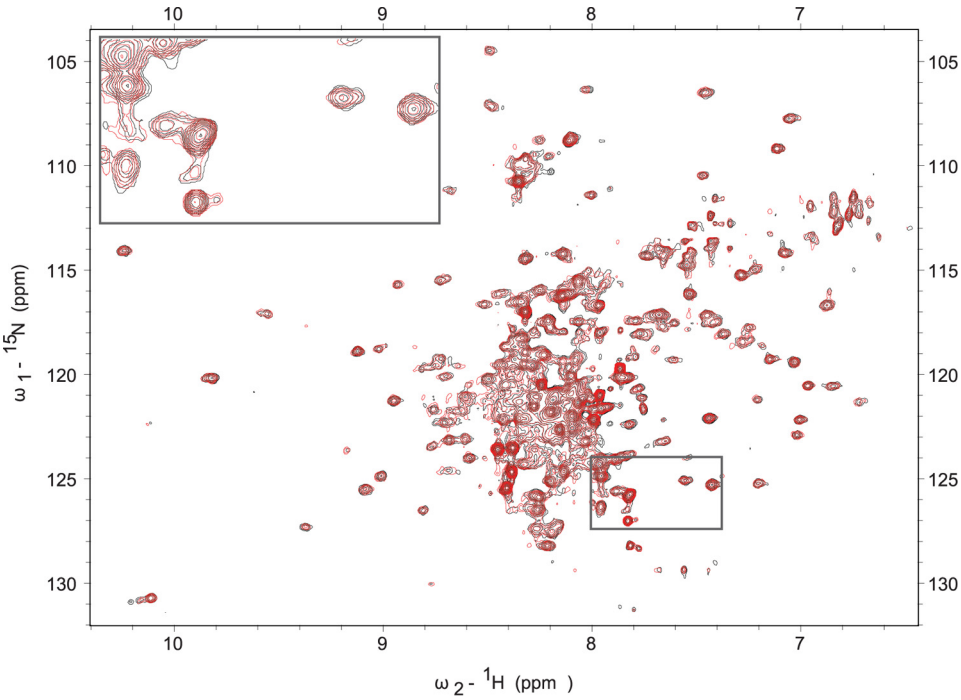

FIGURE 17. **NMR analysis of BVR binding HO-2.** ^{1}H-^{15}N TROSY spectra of 150 μM non-perdeuterated ^{15}N-hHO-2 collected in the absence (*black*) or presence (*red*) of equimolar BVR.

by BVR to undergo conversion to bilirubin. Based on fluorescence quenching, SPR and acetylation protection studies, a moderately tight HO-1·CPR complex with a K_d value in the ~1 μM range had been identified. However, SPR, fluorescence quenching, and acetylation protection assays with HO-1 have yielded inconsistent results regarding which residues form the HO-1/CPR binding interface (24, 25, 27).

Interactions between HO and CPR—Whether or not HO-2 and CPR form a complex has not been previously investigated. As a result of spectroscopic (NMR, fluorescence), steady-state kinetic, and other biochemical (chromatographic, analytical centrifugation, and SPR) studies, we have obtained novel information about the nature of the interactions between these two proteins.

Although our focus is on HO-2, we also analyzed CPR binding to HO-1, primarily as a positive control for the HO-2/CPR studies, as CPR binding HO-1 has been previously described (24–27). Consistent with previous reports, we observe CPR binding HO-1 by SPR and by chemical cross-linking.

By gel filtration experiments, under our experimental conditions (50 μM hHO and 50 μM CPR with $NADP^+$), HO-2 appears to form a homodimer. We do not observe any evidence for a complex between HO-2 and CPR. Gel filtration experiments occur under nonequilibrium conditions in which the component proteins of any transient complex, once dissociated from the complex, are unable to reassociate once they are in a separate zone of the chromatographic column. However, SPR experiments clearly demonstrate CPR binding to HO-2 (Fig. 14).

SPR is a valuable method for studying protein-protein interactions because the proteins remain in the same solution and reach equilibrium; furthermore, one can monitor both the rates of association and dissociation. Our SPR results clearly demonstrate that CPR binds to both HO-1 (K_d = 20.5 μM) and HO-2 (K_d = 16.7 μM) with CPR-dependent rates of association and CPR-independent dissociation rates. For HO-1, our results give a K_d value that is 10-fold larger than previously reported (24). The lower affinity of CPR for HO-1 observed in our studies could be due to differences in the experimental design; our studies were conducted in the absence of heme and utilized immobilized HO-1 with human CPR as the soluble analyte, whereas earlier studies were conducted with immobilized rat CPR with hHO-1 in solution. Although we also observe a binding response when we titrate either hHO-1 or hHO-2 against immobilized human CPR, we found that free heme also produces a strong binding response with immobilized human CPR (Fig. 14*E*) and with immobilized BVR (data not shown). Thus, to avoid potential artifacts, these experiments were performed in the absence of heme. Our use of the apo-HOs is justified by our NMR experiments, which clearly demonstrate that CPR can bind both forms (apoHO-2 and heme-bound) of HO-2. We are unaware of any physiologic rationale for heme binding to CPR, so this is likely to be a nonspecific effect. However, as we discuss below, BVR has previously been shown to bind heme and to shuttle heme into the nucleus (36). Although by SPR we observe no binding of apoHO to immobilized CPR, the conformation of CPR is critical for HO binding (26), and it is possible that immobilization of CPR stabilizes a conformation that has a lower affinity for HO.

Sedimentation velocity experiments also provide evidence of a dynamic complex between HO-2 and CPR, with a K_d (15.1 μM) value that is similar to that calculated from the SPR data. The HO-2·CPR complex can also be captured by chemically cross-linking an amino group of HO-2 through a 15.7 Å tether to a surface-reactive Cys residue on CPR. The latter is, of

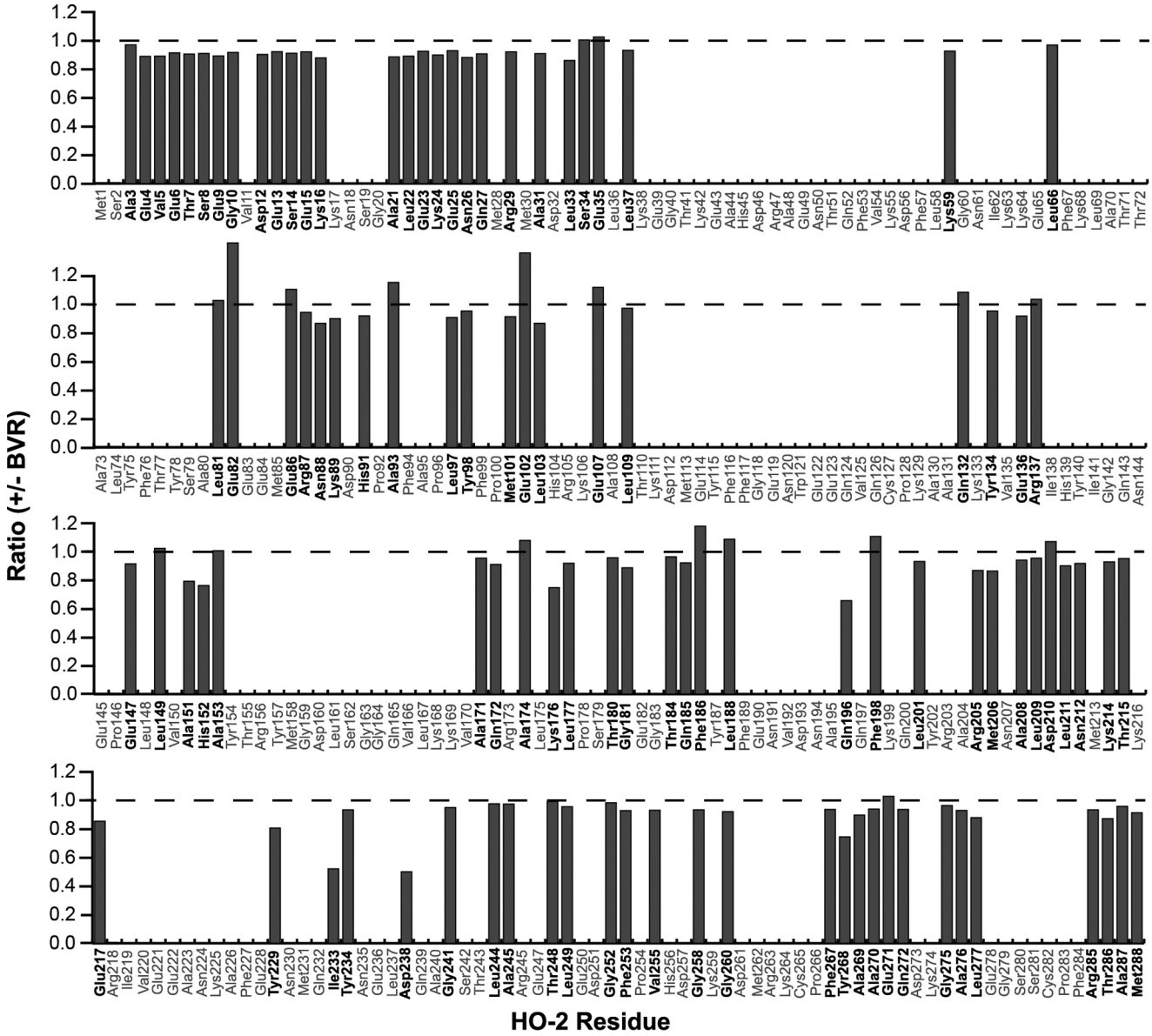

FIGURE 18. **Effect of BVR on HO-2 resonances.** The ratio of hHO-2 resonance height with and without equimolar BVR (*+BVR/−BVR*) is represented by the *gray bars*. A ratio of 1 (*dashed line*) indicates no change for that residue. *Bars* that are absent (*gray labels*) represent resonances that are unassigned, and assigned residues are in *bold*.

course, irreversible and designed to capture even highly transient interactions.

The NMR experiments also show that an interaction between HO-2 and CPR occurs. The primary proof is the overall and large loss of peak intensity for the core resonances, due to broadening associated with the large increase in time-averaged molecular weight. In addition, excess peak intensity loss due to exchange broadening and CSP occurs for several but not all signals. The latter observations are compatible with specific binding and with binding kinetics that are on the fast/intermediate NMR shift time scale ($k_{off} \sim 100\ s^{-1}$). In turn, this is suggestive of a K_d value in the low micromolar range, consistent with the values of 15 μM as found by analytical ultracentrifugation experiments and 16.7 μM as found by SPR. Regretfully, the NMR experiments do not allow a precise determination of these values, because the NMR signals disappear at higher titration stoichiometries, and saturation of binding cannot be observed.

Having assigned ~70% of the resonances in the HO-2 NMR spectrum, we used the CSPs to identify the HO-2/CPR interface. Titration of perdeuterated ^{15}N-hHO-2 with CPR altered the chemical shift of several residues in the hHO-2 NMR spectrum. At both 75 and 150 μM CPR, residues of the HO-2 catalytic core exhibit larger CSPs compared with the N and C termini (Fig. 4). Residues that exhibit the largest CSPs with the addition of 75 μM CPR are Phe-99, Tyr-202, Leu-66, Lys-89, and Glu-190.

Upon adding CPR, we also observed dramatic and titratable reductions in the intensities of some of the ^{1}H-^{15}N TROSY peaks of resonances from the catalytic core domain of HO-2 (Figs. 6 and 9). The majority of intensity changes due to exchange broadening of the TROSY peaks occur in the struc-

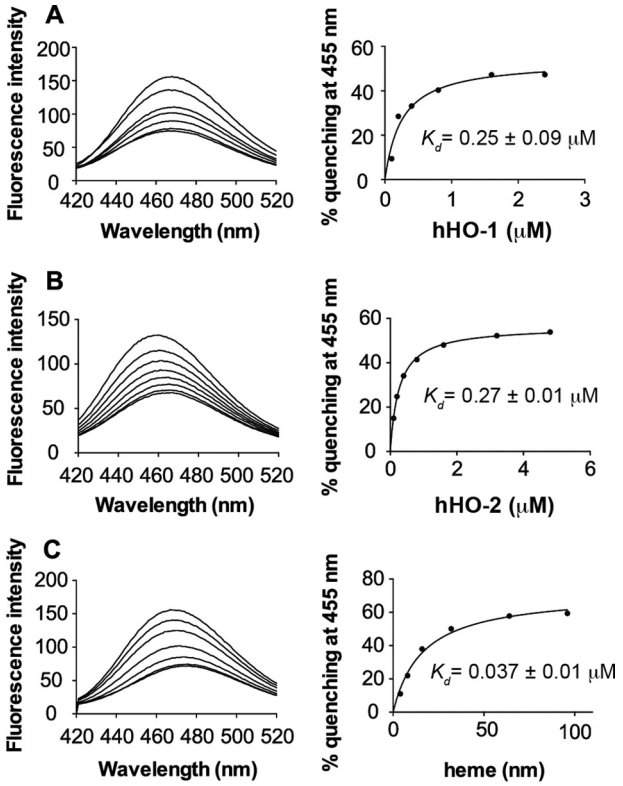

FIGURE 19. **Fluorescence quenching of BVR-CPM by heme oxygenases and heme.** Titration of heme-bound HO-1 (*A*), HO-2 (*B*), or heme alone (*C*) into BVR-CPM. Percent fluorescence quenching plotted against the concentration of the titrant and fit to a single binding model to determine the K_d of binding using GraphPad Prism 6.0.

FIGURE 20. **Biliverdin reductase modified by CPM.** LC-MS/MS analysis of BVR-CPM identifies CPM modification (*) at Cys-280 and either Cys-292 or Cys-293. Cys-74 was not observed in this analysis.

tured core region of HO-2, with few intensity changes originating from the dynamically unfolded N (Ser-8) or C terminus (Tyr-268). Chemical shift perturbations induced by CPR titrations also affect the core residues of hHO-2, although the N and C termini are unaffected (Fig. 4). These results indicate that CPR interacts with the catalytic core of the protein and has minimal interactions with the N- or C-terminal regions of HO-2.

Fig. 22*A* highlights residues on hHO-2 that exhibit *both* significant CSPs and large intensity changes with the addition of 75 μM CPR as follows: Leu-66, Phe-99, Glu-102, Asp-193, Gln-200, Tyr-202, and Leu-209. Strikingly, in the recent HO-1/CPR crystal structure, residues conserved with HO-2, Phe-99, Glu-102, Gln-200, and Tyr-202 form a patch that is at the CPR interface (Fig. 22*B*). The HO-1 residue conserved with Asp-193 is also located at the CPR interface, as are HO-1 residues conserved with the HO-2 residues targeted by mutagenesis, Leu-201 and Lys-169 (Fig. 22).

Additional HO-2 residues show either significant CSPs without extra intensity change or large changes in intensity without chemical shift changes. Especially the latter phenomenon is

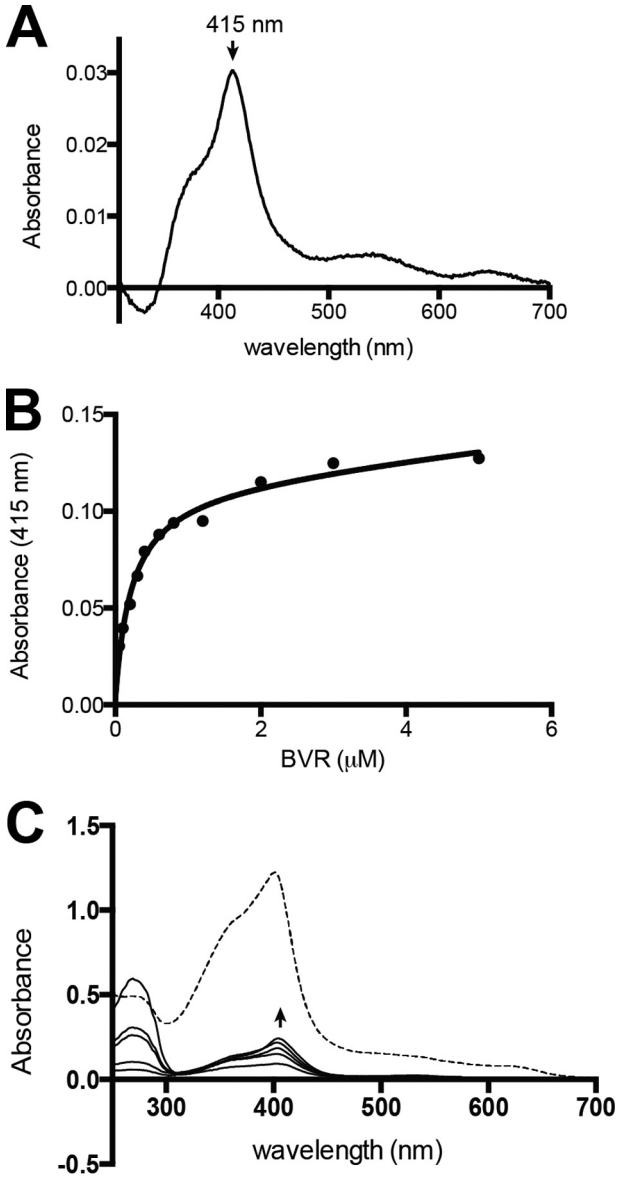

FIGURE 21. **Heme binds BVR by optical absorbance.** *A,* absorbance spectrum of 2.5 μM BVR with 2.0 μM heme. BVR alone shows no absorbance in the 350–700 nm range. *B,* A_{414} of 10 μM heme titrated with varying concentrations of BVR (0.05, 0.1, 0.2, 0.3, 0.4, 0.6, 0.8, 1.2, 2.0, 3.0, and 5.0 μM BVR). Data are fit to a single binding model using GraphPad Prism 6.0. *C,* 5 μM hHO-2 alone (*dotted line*) or titrated with various concentrations of BVR (1.0, 2.0, 8.0, 10.0, and 20.0 μM). Samples for BVR titrations contain 5 μM hHO-2 in the reference cuvette because the absorbance of hHO-2 is ~10-fold that of heme-BVR, and the hHO-2 spectrum overwhelms the heme-BVR spectrum if it is not subtracted.

prevalent for the most affected residue, Leu-201, and is theoretically incompatible with a canonical intermediate exchange binding process as described by Equation 2. Rather, it is suggestive of additional, significantly populated bound states of CPR sensed by Leu-201 that are in intermediate/fast exchange with each other and with Leu-201 in the free state. It can be shown that the observed broadening without shift can occur if the CSPs of the different bound states approximately cancel.[6] The residues affected by this noncanonical mechanism are conserved in HO-1, where they are located at the interface for CPR

[6] E. R. P. Zuiderweg, unpublished data.

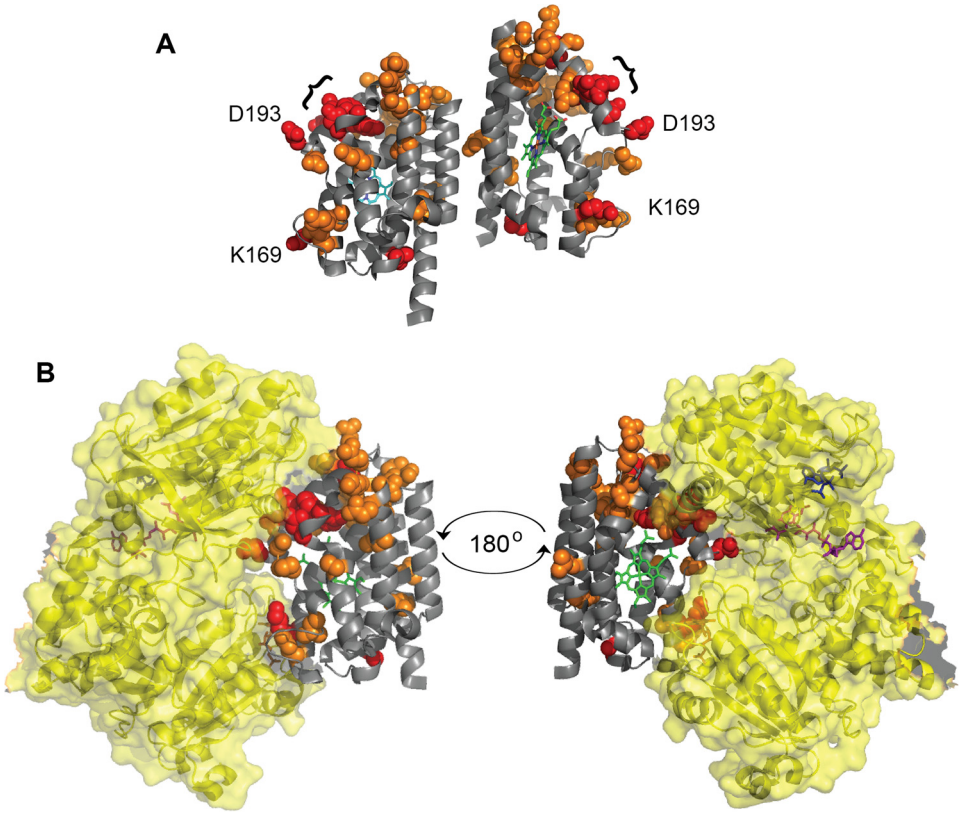

FIGURE 22. **Interface for CPR on HO-2 defined by NMR and mutagenesis.** *A,* residues in *red* have *both* significant CSPs and large intensity ratio changes with the addition of 75 μM CPR. Residues of HO-2 that have significant CSPs *or* large changes in peak intensity ratio with the addition of 75 μM CPR are shown in *orange*. { identifies a patch of residues strongly affected by CPR (Phe-99, Glu-102, Gln-200, Leu-201, and Tyr-202). Leu-201 and Lys-169 were identified by mutagenesis. Side chains are shown as *spheres* (PDB 2QPP). *B,* residues identified for HO-2 mapped onto the analogous residues of HO-1 in the published crystal structure of the complex of rat HO-1 (*gray*) and rat CPRΔTGEE (*yellow*) (PDB 3WKT). Cofactors are as indicated as follows: heme (*green*), $NADP^+$ (*blue*), FAD (*purple*), and FMN (*orange*).

(Glu-86, Asp-90, Glu-190, Leu-201, Arg-203, Ala-208, and Asp-210) or in patches of residues adjacent to the interface in (Ala-31, Leu-33, Leu-36, Leu-37, Leu-81, Glu-107, Lys-89, Asn-88, Leu-149, Gln-172, Glu-182, Thr-184, and Thr-215). These residues also localize at and around the binding site for HO-2 as identified from CSPs alone. The extended nature of the interaction surface would also be compatible with multiple binding modes for CPR as implied from the noncanonical broadening. The existence of multiple bound states, or an ensemble of encounter complexes, has been suggested for other electron transfer complexes as well (60, 61).

NMR relaxation and gel filtration studies indicate that HO-2 exists as a homodimer in solution at the conditions used. Changes in the homodimerization state of HO-2 upon CPR binding could give rise to CPR-dependent changes in the TROSY spectrum, and these changes would be difficult to distinguish from changes induced by CPR binding HO-2 directly. However, HO-2 crystallizes as a homodimer, and the HO-2/HO-2 interface is distant from the majority of the CPR-induced changes that occur in the HO-2 TROSY spectrum (Fig. 22*A*). This supports that the CPR-induced changes observed in the HO-2 TROSY spectrum are not due to changes in the HO-2 dimerization state but rather CPR directly binding to HO-2.

There is a major difference between the k_{off} as suggested by NMR ($\sim$100 s^{-1}) and the value measured by SPR ($\sim$0.023 s^{-1}). The latter value would give rise to an extremely slow NMR shift time scale and would not allow for any of the observed chemical shift changes. This contradictory situation is reminiscent of the binding of an organic phosphate molecule to hemoglobin, where, despite an off-rate of 0.01 s^{-1}, fast exchange dynamics were observed using ^{31}P NMR. Multiple binding sites for the small molecule on the hemoglobin surface were proposed to explain the apparent discrepancy, and a mathematical model that recapitulated the experimental results was described (62, 63). In this study, we have evidence for the existence of multiple bound states of CPR. Perhaps the observed rate of $\sim$100 s^{-1} as indicated by NMR is reflective of the exchange kinetics between the various bound states. In contrast, the off-rate as measured by SPR monitors the complete dissociation.

Although previous reports on the HO-1·CPR complex focus on charge-charge interactions (from residues that we were not able to assign in our NMR spectra), our results provide the first evidence that hydrophobic residues may be involved in HO/CPR binding. The majority of the residues highlighted in the NMR binding studies are involved in interacting with the FAD binding domain of CPR (Fig. 22). Kinetic results discussed below concur with these NMR results.

Our steady-state kinetic analyses support the conclusion that the area near the exposed heme binding face in the catalytic core of HO-2 is involved in binding CPR. For example, HO-1 and HO-2, which share a high degree of structural similarity in their catalytic core region (55), exhibit similar K_m values for

CPR (0.5–0.7 μM). Furthermore, alanine substitution of the core residues that are proposed to be at the HO/CPR interface, Lys-169 (or Lys-149 in HO-1) and Leu-201, results in significant increases in the K_m value for CPR. K169A, for example, exhibits a 20-fold increase in K_m for CPR, in close agreement with prior SPR (24) and acetylation protection assays (25) but in contrast with earlier FRET measurements, which showed no effect of Ala substitution at that site (27). The K169A variant of HO-2 also exhibits a 1.4-fold increase in V_{max}, and the K149A variant of HO-1 exhibits a 2.2-fold increase in V_{max} suggesting that lowering the affinity for CPR increases the steady-state rate under saturating substrate (NADPH, O_2, and CPR) concentrations. That the K149A variant binds heme with identical affinity as the wild type (24) and does not exhibit a decrease (instead a slight increase) in V_{max} supports our conclusion that its increase in K_m for CPR reflects disruption of a key interaction between CPR and HO-2, not some major disruption in the overall structure or at the active site.

The HO reaction involves many steps, including heme binding, seven steps of electron transfer, 3 mol of oxygen binding, oxygen activation, biliverdin release, etc. It is accepted that the rate-limiting step in the HO-1 catalytic cycle when BVR is present is the ring opening of Fe(II)-verdoheme (40, 64). However, it is possible that this lysine variant is rate-limited by another step. The details of the catalytic cycle for HO-2 or for this variant have not been characterized. However, given that K149A (HO-1) and K169A (HO-2) exhibit a 1.4–2.2-fold increase in V_{max} and a 20–40-fold increase in K_m for CPR, it seems reasonable to speculate that, at saturating concentrations of CPR, the rate-limiting step for this lysine variant is electron transfer from CPR to the heme.

Taken together, our results suggest that during the multistep HO-2 reaction, a transient complex between HO-2 and CPR forms and dissociates rapidly and that the productive electron transfer complex includes HO-2 residues Leu-201 and Lys-169. The transient nature of the interactions between HO-2 and CPR is likely to be an important catalytic feature, especially in this and other systems where multiple electrons must be passed during each catalytic cycle.

Our results indicate that a similar dynamic and transient binding scenario exists with HO-1. Our gel filtration and SPR results indicate that HO-1 (like HO-2) forms a rather weak complex with CPR. The transient nature of these interactions between HO and CPR is likely to be important in the HO mechanism, which requires seven electrons to be transferred from NADPH through the redox centers on CPR.

The catalytic core, shown clearly to be the domain of HO-2 that interacts with CPR, is highly homologous with HO-1. For example, catalytic core residues with NMR resonances most strongly affected by CPR that exhibit both CSPs and broadening (Leu-66, Phe-99, Glu-102, Asp-193, Gln-200, Tyr-202, and Leu-209) or with binding constants affected by mutagenesis (Lys-169 and Leu-201) are highly conserved between HO-1 and HO-2. All of those residues are strictly conserved except Leu-66 (Gly-46 in HO-1). Earlier reports identified Lys-149 of HO-1 to be important in binding CPR (24, 25). It was shown that CPR prevents acetylation of that Lys residue and that substitution of Ala at that position results in a 7-fold decrease in affinity for CPR. We found that the K149A substitution results in a 40-fold increase in K_m for CPR (20-fold for the analogous K169A mutation in HO-2). Thus, it appears that both HOs interact similarly with CPR.

Our results support that HO-2 forms a highly dynamic complex with CPR at an interface that includes HO-2 residues Leu-201 and Lys-169, and the CPR interface is likely highly conserved for both HO-1 and HO-2. As shown in Fig. 22*B*, the homologous residues in HO-1 (Leu-181 and Lys-149) are located at the HO-1/CPR interface in the crystal structure of a complex between HO-1 and a deletion variant of CPR (CPR ΔTGEE) (26). This CPR variant forms a stable complex with HO-1 that, unlike the wild type protein, can be observed even by gel filtration (26). Given the high homology of the structures of the catalytic cores of HO-1 and HO-2 (55), we suggest that Leu-201 and Lys-169 of HO-2 participate in stabilizing the electron transfer complex between HO-2 and CPR.

Interactions between HO and BVR—Based on prior fluorescence quenching studies, HO-1 and BVR were proposed to form a high affinity complex (27), and our goal was to characterize the analogous HO-2·BVR complex using various biochemical and biophysical methods. However, addition of BVR to ^{15}N-labeled hHO-2 results in no chemical shift perturbation and, of the 104 assigned resonances in the hHO-2 spectrum, only five exhibit a BVR-dependent decrease in intensity. Of those residues that exhibit sensitivity to BVR, three are on the surface of the crystal structure and could reasonably be involved in binding BVR (Lys-176, Gln-196, and Tyr-229) (Fig. 18). In contrast, under the same conditions with equimolar CPR, 48 of the assigned HO-2 resonances exhibit strong CPR-dependent effects (Fig. 9). These results suggest BVR binds hHO-2 with a weak affinity compared with CPR.

Because the TROSY experiments indicated that HO-2 does not bind BVR with high affinity (Fig. 18), we repeated the original fluorescence quenching studies that described the hHO-1·BVR complex (27). Although our results with hHO-1 are nearly identical to those described in the original paper, additional controls indicate that free heme strongly quenches BVR-CPM fluorescence independently of HO. We also used optical absorbance methods to verify the ability of BVR to bind heme, as was reported previously (36). The K_d value for the heme·BVR complex differs between the two experiments, with the absorbance data indicating binding of more than heme to BVR. Furthermore, labeled BVR contains fluorophores at two specific sites (Cys-292 or Cys-293 and Cys-204). We suggest that the fluorescence quenching studies may monitor binding of one heme to BVR at a high affinity site near one of these fluorophores, although the optical absorbance studies may reflect multiple heme binding events.

Thus, the fluorescence quenching studies aimed at studying interactions between HO-2 and BVR actually report on binding of heme in solution that has dissociated from hHO, rather than direct interactions between hHO and BVR. In fact, detection of an HO·BVR complex requires the use of methods like chemical cross-linking, where even transient complexes can be trapped.

This result describing the low affinity of HO for BVR is important because it clarifies the mechanism by which BVR couples to the HO reaction. It has been shown that BVR

changes the rate-limiting step of the HO-1 reaction from biliverdin release to the conversion of the Fe^{2+}-verdoheme intermediate to Fe^{3+}-biliverdin (40). We had taken this to indicate the possibility that biliverdin is channeled between the two proteins. However, it now appears that the effect of BVR on the HO rate-limiting step occurs by kinetic coupling of the HO and BVR reactions, not substrate channeling. BVR binds HO-2 very weakly; therefore, substrate channeling, which requires a stable complex, is unlikely. Thus, BVR simply binds the biliverdin upon release from its product complex with HO, enhancing the HO reaction by affecting the mass balance.

Conclusions—In conclusion, we show that protein·protein complexes between HO-2 and other proteins in the heme degradation pathway (CPR and BVR) are highly transient. HO-2 and CPR form a transient electron transfer complex and, like other electron transfer pairs, HO-2 and CPR may form an ensemble of complexes that is in equilibrium with the productive electron transfer complex. NMR binding studies and mutagenesis of HO-2 highlight an interface for CPR on HO-2, which is consistent with what has been described for CPR and HO-1. However, in contrast to studies with CPR and HO-1, our results suggest that CPR binding HO-2 in solution is dynamic. Gel filtration and ultracentrifugation studies support a weak/transient CPR·HO-2 complex. Complex formation between HO-2 and BVR is undetected, except via irreversible binding (cross-linking) methods. In the cell, CPR is an electron donor for many biologically important reactions. The dynamic interactions between CPR and HO-2 revealed in these studies may play an important role in the regulation of the HO system in a cellular context.

REFERENCES

1. Sassa, S. (2004) Why heme needs to be degraded to iron, biliverdin IXα, and carbon monoxide? *Antioxid. Redox Signal.* **6,** 819–824
2. Furuyama, K., Kaneko, K., and Vargas, P. D. (2007) Heme as a magnificent molecule with multiple missions: heme determines its own fate and governs cellular homeostasis. *Tohoku J. Exp. Med.* **213,** 1–16
3. Maines, M. D. (2004) The heme oxygenase system: past, present, and future. *Antioxid. Redox Signal.* **6,** 797–801
4. Maines, M. D. (2005) The heme oxygenase system: update 2005. *Antioxid. Redox. Signal.* **7,** 1761–1766
5. Maines, M. D. (1993) Carbon monoxide: an emerging regulator of cGMP in the brain. *Mol. Cell. Neurosci.* **4,** 389–397
6. Kim, H. P., Ryter, S. W., and Choi, A. M. (2006) CO as a cellular signaling molecule. *Annu. Rev. Pharmacol. Toxicol.* **46,** 411–449
7. Hanafy, K. A., Oh, J., and Otterbein, L. E. (2013) Carbon monoxide and the brain: time to rethink the dogma. *Curr. Pharm. Des.* **19,** 2771–2775
8. Andrews, N. C., and Schmidt, P. J. (2007) Iron homeostasis. *Annu. Rev. Physiol.* **69,** 69–85
9. Jansen, T., Hortmann, M., Oelze, M., Opitz, B., Steven, S., Schell, R., Knorr, M., Karbach, S., Schuhmacher, S., Wenzel, P., Münzel, T., and Daiber, A. (2010) Conversion of biliverdin to bilirubin by biliverdin reductase contributes to endothelial cell protection by heme oxygenase-1-evidence for direct and indirect antioxidant actions of bilirubin. *J. Mol. Cell. Cardiol.* **49,** 186–195
10. Baranano, D. E., Rao, M., Ferris, C. D., and Snyder, S. H. (2002) Biliverdin reductase: a major physiologic cytoprotectant. *Proc. Natl. Acad. Sci. U.S.A.* **99,** 16093–16098
11. Sedlak, T. W., Saleh, M., Higginson, D. S., Paul, B. D., Juluri, K. R., and Snyder, S. H. (2009) Bilirubin and glutathione have complementary antioxidant and cytoprotective roles. *Proc. Natl. Acad. Sci. U.S.A.* **106,** 5171–5176
12. McCoubrey, W. K., Jr., Huang, T. J., and Maines, M. D. (1997) Isolation and characterization of a cDNA from the rat brain that encodes hemoprotein heme oxygenase-3. *Eur. J. Biochem.* **247,** 725–732
13. Hayashi, S., Omata, Y., Sakamoto, H., Higashimoto, Y., Hara, T., Sagara, Y., and Noguchi, M. (2004) Characterization of rat heme oxygenase-3 gene. Implication of processed pseudogenes derived from heme oxygenase-2 gene. *Gene* **336,** 241–250
14. Ishikawa, K., Takeuchi, N., Takahashi, S., Matera, K. M., Sato, M., Shibahara, S., Rousseau, D. L., Ikeda-Saito, M., and Yoshida, T. (1995) Heme oxygenase-2. Properties of the heme complex of the purified tryptic fragment of recombinant human heme oxygenase-2. *J. Biol. Chem.* **270,** 6345–6350
15. Maines, M. D. (1997) The heme oxygenase system: a regulator of second messenger gases. *Annu. Rev. Pharmacol. Toxicol.* **37,** 517–554
16. Huang, T. J., McCoubrey, W. K., Jr., and Maines, M. D. (2001) Heme oxygenase-2 interaction with metalloporphyrins: function of heme regulatory motifs. *Antioxid. Redox Signal.* **3,** 685–696
17. Yi, L., and Ragsdale, S. W. (2007) Evidence that the heme regulatory motifs in heme oxygenase-2 serve as a thiol/disulfide redox switch regulating heme binding. *J. Biol. Chem.* **282,** 21056–21067
18. Yi, L., Jenkins, P. M., Leichert, L. I., Jakob, U., Martens, J. R., and Ragsdale, S. W. (2009) Heme regulatory motifs in heme oxygenase-2 form a thiol/disulfide redox switch that responds to the cellular redox state. *J. Biol. Chem.* **284,** 20556–20561
19. Varfaj, F., Lampe, J. N., and Ortiz de Montellano, P. R. (2012) Role of cysteine residues in heme binding to human heme oxygenase-2 elucidated by two-dimensional NMR spectroscopy. *J. Biol. Chem.* **287,** 35181–35191
20. Strobel, H. W., Hodgson, A. V., and Shen., S. (1995) in *Cytochrome P450* (Ortiz de Montellano, P. R., ed) pp. 225–244, Springer-Verlag Inc., New York
21. Tenhunen, R., Marver, H. S., and Schmid, R. (1969) Microsomal heme oxygenase. Characterization of the enzyme. *J. Biol. Chem.* **244,** 6388–6394
22. Yoshida, T., Noguchi, M., and Kikuchi, G. (1980) Inability of the NADH-cytochrome b5 reductase system to initiate heme degradation yielding biliverdin IX α from the oxygenated form of heme. heme oxygenase complex. *FEBS Lett.* **115,** 278–280
23. Kenaan, C., Zhang, H., Shea, E. V., and Hollenberg, P. F. (2011) Uncovering the role of hydrophobic residues in cytochrome P450-cytochrome P450 reductase interactions. *Biochemistry* **50,** 3957–3967
24. Higashimoto, Y., Sakamoto, H., Hayashi, S., Sugishima, M., Fukuyama, K., Palmer, G., and Noguchi, M. (2005) Involvement of NADPH in the interaction between heme oxygenase-1 and cytochrome P450 reductase. *J. Biol. Chem.* **280,** 729–737
25. Higashimoto, Y., Sugishima, M., Sato, H., Sakamoto, H., Fukuyama, K., Palmer, G., and Noguchi, M. (2008) Mass spectrometric identification of lysine residues of heme oxygenase-1 that are involved in its interaction with NADPH-cytochrome P450 reductase. *Biochem. Biophys. Res. Commun.* **367,** 852–858
26. Sugishima, M., Sato, H., Higashimoto, Y., Harada, J., Wada, K., Fukuyama, K., and Noguchi, M. (2014) Structural basis for the electron transfer from an open form of NADPH-cytochrome P450 oxidoreductase to heme oxygenase. *Proc. Natl. Acad. Sci. U.S.A.* **111,** 2524–2529
27. Wang, J., and de Montellano, P. R. (2003) The binding sites on human heme oxygenase-1 for cytochrome p450 reductase and biliverdin reductase. *J. Biol. Chem.* **278,** 20069–20076
28. Danielson, P. B. (2002) The cytochrome P450 superfamily: biochemistry, evolution and drug metabolism in humans. *Curr. Drug Metab.* **3,** 561–597
29. Enoch, H. G., and Strittmatter, P. (1979) Cytochrome *b*5 reduction by NADPH-cytochrome P-450 reductase. *J. Biol. Chem.* **254,** 8976–8981
30. Williams, C. H., Jr., and Kamin, H. (1962) Microsomal triphosphopyridine nucleotide-cytochrome c reductase of liver. *J. Biol. Chem.* **237,** 587–595
31. Ono, T., and Bloch, K. (1975) Solubilization and partial characterization of rat liver squalene epoxidase. *J. Biol. Chem.* **250,** 1571–1579
32. Linnenbaum, M., Busker, M., Kraehling, J. R., and Behrends, S. (2012) Heme oxygenase isoforms differ in their subcellular trafficking during hypoxia and are differentially modulated by cytochrome P450 reductase. *PLoS One* **7,** e35483
33. Kutty, R. K., and Maines, M. D. (1981) Purification and characterization of

biliverdin reductase from rat liver. *J. Biol. Chem.* **256,** 3956–3962
34. Maines, M. D., Ewing, J. F., Huang, T. J., and Panahian, N. (2001) Nuclear localization of biliverdin reductase in the rat kidney: response to nephrotoxins that induce heme oxygenase-1. *J. Pharmacol. Exp. Ther.* **296,** 1091–1097
35. Ahmad, Z., Salim, M., and Maines, M. D. (2002) Human biliverdin reductase is a leucine zipper-like DNA-binding protein and functions in transcriptional activation of heme oxygenase-1 by oxidative stress. *J. Biol. Chem.* **277,** 9226–9232
36. Tudor, C., Lerner-Marmarosh, N., Engelborghs, Y., Gibbs, P. E., and Maines, M. D. (2008) Biliverdin reductase is a transporter of haem into the nucleus and is essential for regulation of HO-1 gene expression by haematin. *Biochem. J.* **413,** 405–416
37. Miralem, T., Hu, Z., Torno, M. D., Lelli, K. M., and Maines, M. D. (2005) Small interference RNA-mediated gene silencing of human biliverdin reductase, but not that of heme oxygenase-1, attenuates arsenite-mediated induction of the oxygenase and increases apoptosis in 293A kidney cells. *J. Biol. Chem.* **280,** 17084–17092
38. Lerner-Marmarosh, N., Shen, J., Torno, M. D., Kravets, A., Hu, Z., and Maines, M. D. (2005) Human biliverdin reductase: A member of the insulin receptor substrate family with serine/threonine/tyrosine kinase activity. *Proc. Natl. Acad. Sci. U.S.A.* **102,** 7109–7114
39. Lerner-Marmarosh, N., Miralem, T., Gibbs, P. E., and Maines, M. D. (2008) Human biliverdin reductase is an ERK activator; hBVR is an ERK nuclear transporter and is required for MAPK signaling. *Proc. Natl. Acad. Sci. U.S.A.* **105,** 6870–6875
40. Liu, Y., and Ortiz de Montellano, P. R. (2000) Reaction intermediates and single turnover rate constants for the oxidation of heme by human heme oxygenase-1. *J. Biol. Chem.* **275,** 5297–5307
41. Aslanidis, C., and de Jong, P. J. (1990) Ligation-independent cloning of PCR products (LIC-PCR). *Nucleic Acids Res.* **18,** 6069–6074
42. Marohnic, C. C., Panda, S. P., Martásek, P., and Masters, B. S. (2006) Diminished FAD binding in the Y459H and V492E Antley-Bixler syndrome mutants of human cytochrome P450 reductase. *J. Biol. Chem.* **281,** 35975–35982
43. Dawson, R. M. C., Elliott, D. C., Elliott, W. H., and Jones, K. M. (1986) *Data for Biochemical Research*, 3rd Ed., Clarendon Press, London
44. Delaglio, F., Grzesiek, S., Vuister, G. W., Zhu, G., Pfeifer, J., and Bax, A. (1995) NMRPipe: a multidimensional spectral processing system based on UNIX pipes. *J. Biomol. NMR* **6,** 277–293
45. Goddard, T. D., and Kneller, D. G. (2008) *SPARKY 3*, Version 3.1115, University of California, San Francisco
46. Andresen, C., Helander, S., Lemak, A., Farès, C., Csizmok, V., Carlsson, J., Penn, L. Z., Forman-Kay, J. D., Arrowsmith, C. H., Lundström, P., and Sunnerhagen, M. (2012) Transient structure and dynamics in the disordered c-Myc transactivation domain affect Bin1 binding. *Nucleic Acids Res.* **40,** 6353–6366
47. Cavanagh, J., Fairbrother, W. J., and Palmer, A. G., III, Rance, M., and Skelton, N. J. (2006) *Protein NMR Spectroscopy: Principles and Practice*, 2nd Ed., Elsevier Academic Press, San Diego
48. Quenouille, M. H. (1956) Notes on bias in estimation. *Biometrika* **43,** 353–360
49. Ishikawa, K., Matera, K. M., Zhou, H., Fujii, H., Sato, M., Yoshimura, T., Ikeda-Saito, M., and Yoshida, T. (1998) Identification of histidine 45 as the axial heme iron ligand of heme oxygenase-2. *J. Biol. Chem.* **273,** 4317–4322
50. Huber, W. J., 3rd, Marohnic, C. C., Peters, M., Alam, J., Reed, J. R., Masters, B. S., and Backes, W. L. (2009) Measurement of membrane-bound human heme oxygenase-1 activity using a chemically defined assay system. *Drug Metab. Dispos.* **37,** 857–864
51. Dam, J., Velikovsky, C. A., Mariuzza, R. A., Urbanke, C., and Schuck, P. (2005) Sedimentation velocity analysis of heterogeneous protein-protein interactions: Lamm equation modeling and sedimentation coefficient distributions $c(s)$. *Biophys. J.* **89,** 619–634
52. Schuck, P. (2000) Size-distribution analysis of macromolecules by sedimentation velocity ultracentrifugation and Lamm equation modeling. *Biophys. J.* **78,** 1606–1619
53. Sambrook, J., and Russell, D. (2001) *Molecular Cloning: A Laboratory Manual*, 3rd Ed., Cold Spring Harbor Laboratory Press, Cold Spring Harbor, NY
54. Pervushin, K., Riek, R., Wider, G., and Wüthrich, K. (1997) Attenuated T2 relaxation by mutual cancellation of dipole-dipole coupling and chemical shift anisotropy indicates an avenue to NMR structures of very large biological macromolecules in solution. *Proc. Natl. Acad. Sci. U.S.A.* **94,** 12366–12371
55. Bianchetti, C. M., Yi, L., Ragsdale, S. W., and Phillips, G. N., Jr. (2007) Comparison of apo- and heme-bound crystal structures of a truncated human heme oxygenase-2. *J. Biol. Chem.* **282,** 37624–37631
56. Baker, J. M., Hudson, R. P., Kanelis, V., Choy, W. Y., Thibodeau, P. H., Thomas, P. J., and Forman-Kay, J. D. (2007) CFTR regulatory region interacts with NBD1 predominantly via multiple transient helices. *Nat. Struct. Mol. Biol.* **14,** 738–745
57. Carrington, A., and MacLachlan, A. (1967) *Introduction to Magnetic Resonance with Applications to Chemistry and Chemical Physics*, Harper & Row, New York
58. Tanford, C. (1963) *Physical Chemistry of Macromolecules,* John Wiley & Sons, Inc., New York
59. McCoubrey, W. K., Jr., and Maines, M. D. (1994) Site-directed mutagenesis of cysteine residues in biliverdin reductase. Roles in substrate and cofactor binding. *Eur. J. Biochem.* **222,** 597–603
60. Crowley, P. B., and Ubbink, M. (2003) Close encounters of the transient kind: protein interactions in the photosynthetic redox chain investigated by NMR spectroscopy. *Acc. Chem. Res.* **36,** 723–730
61. Ubbink, M. (2009) The courtship of proteins: understanding the encounter complex. *FEBS Lett.* **583,** 1060–1066
62. Zuiderweg, E. R., Hamers, L. F., Rollema, H. S., de Bruin, S. H., and Hilbers, C. W. (1981) ^{31}P NMR study of the kinetics of binding of myo-inositol hexakisphosphate to human hemoglobin. Observation of fast-exchange kinetics in high affinity systems. *Eur. J. Biochem.* **118,** 95–104
63. Zuiderweg, E. R. (2012) in *Recent Developments in Biomolecular NMR* (Clore, G., and Potts, J., eds) pp. 216–252, Royal Society of Chemistry, Cambridge, UK
64. Matsui, T., Unno, M., and Ikeda-Saito, M. (2010) Heme oxygenase reveals its strategy for catalyzing three successive oxygenation reactions. *Acc. Chem. Res.* **43,** 240–247